scientific reports

Check for updates

OPEN

The superior performance of silica gel supported nano zero-valent iron for simultaneous removal of Cr (VI)

Eslam Salama[1], Mahmoud Samy[2], Hassan Shokry[3,4], Gehan El-Subruiti[5], Asmaa El-Sharkawy[5], Hesham Hamad[6]✉ & Marwa Elkady[6,7]✉

Pure nano zero-valent iron (NZVI) was fabricated under optimum conditions based on material production yield and its efficiency toward acid blue dye-25 decolorization. The optimum prepared bare NZVI was immobilized with two different supports of silica and starch to fabricate their composites nanomaterials. The three different prepared zero-valent iron-based nanomaterials were evaluated for removal of hexavalent chromium (Cr(VI)). The silica-modified NZVI recorded the most outstanding removal efficiency for Cr(VI) compared to pristine NZVI and starch-modified NZVI. The removal efficiency of Cr(VI) was improved under acidic conditions and decreased with raising the initial concentration of Cr(VI). The co-existence of cations, anions, and humic acid reduced Cr(VI) removal efficiency. The removal efficiency was ameliorated from 96.8% to 100% after adding 0.75 mM of H_2O_2. The reusability of silica-modified NZVI for six cycles of Cr(VI) removal was investigated and the removal mechanism was suggested as the physicochemical process. Based on Langmuir isotherm, the maximal Cr(VI) removal capacity attained 149.25 mg/g. Kinetic and equilibrium data were efficiently fitted using the pseudo-second-order and Langmuir models, respectively confirming the proposed mechanism. Diffusion models affirmed that the adsorption rate was governed by intraparticle diffusion. Adsorption thermodynamic study suggested the spontaneity and exothermic nature of the adsorption process. This study sheds light on the technology that has potential for magnetic separation and long-term use for effective removal of emerging water pollutants.

Chromium ions and dyes can be released with the industrial effluents of various industries such as steel, electroplating, textile, tannery, leather, paper, food and cosmetics[1,2]. The presence of chromium ions and dyes in surface and groundwater has negative impacts on living organisms due to their high toxicity, carcinogenicity, and biorecalcitrance[3,4]. Chromium is a heavy metal that frequently exists in two forms (trivalent [Cr(III)] and hexavalent [Cr(VI)])[5]. Cr(VI) is featured by its higher toxicity, solubility, and mobility compared to Cr(III)[6]. The existence of Cr(VI) ions in the human body can result in severe risks such as skin disease, diabetes and respiratory problems[7]. Moreover, it can destroy RNA and DNA[8]. The permissible concentration of Cr(VI) in the industrial effluents before the discharge to surface water is less than 0.05 mg L^{-1} according to international standards[9]. Moreover, dyes are characterized by their high color strength affecting negatively the photosynthesis

[1]Environment and Natural Materials Research Institute (ENMRI), City of Scientific Research and Technological Applications (SRTA-City), New Borg El-Arab City, Alexandria 21934, Egypt. [2]Department of Public Works Engineering, Faculty of Engineering, Mansoura University, Mansoura 35516, Egypt. [3]Environmental Engineering Department, Egypt-Japan University of Science and Technology (E-JUST), New Borg El-Arab City, Alexandria, Egypt. [4]Electronic Materials Research Department, Advanced Technology and New Materials Research Institute, City of Scientific Research and Technological Applications (SRTA-City), New Borg El-Arab City, Alexandria 21934, Egypt. [5]Chemistry Department, Faculty of Science, Alexandria University, Ibrahimia, Alexandria, Egypt. [6]Fabrication Technology Research Department, Advanced Technology and New Materials Research Institute, City of Scientific Research and Technological Applications (SRTA-City), New Borg El-Arab City, Alexandria 21934, Egypt. [7]Chemical and Petrochemical Engineering Department, Egypt-Japan University of Science and Technology (E-JUST), New Borg El-Arab City, Alexandria 21934, Egypt. ✉email: heshamaterials@hotmail.com; hhamad@srtacity.sci.eg; marwa.f.elkady@gmail.com

process[10]. Therefore, the industrial effluents containing Cr(VI) or/and dyes have to receive an effective treatment before their release into aquatic systems.

Various techniques such as photocatalysis, chemical precipitation, membrane filtration, coagulation and biological processes have been employed for the removal of Cr(VI) and dyes[11–16]. However, the aforementioned techniques have some defects such as the low removal performance, high cost and generation of secondary contaminants[17–19]. The adsorption process combined with chemical reduction is a promising technique due to its simplicity, low-cost and high removal performance towards various pollutants[20]. Moreover, the secondary pollutants generated via this process are limited[21]. Recently, nano zero-valent iron (NZVI) has been evaluated as an adsorbent owing to its inexpensiveness, high removal capacity, availability, facile preparation and high surface area[22,23]. Furthermore, NZVI can reduce dyes to less toxic compounds and Cr(VI) to Cr(III)[24]. The preparation of NZVI using different reducing agents and iron precursors under different reaction times can greatly affect the yield and removal performance of NZVI. Therefore, the optimization of the preparation of NZVI under the aforementioned factors was conducted based on the yield and the removal performance of acid blue-25 dye. Despite the aforementioned excellent characteristics of NZVI, it can easily aggregate because of its magnetic properties and van der Waals forces which adversely affect the reactivity and reducibility performance of NZVI[25]. Additionally, oxidation of NZVI can frequently take place leading to the formation of a corrosion layer on its surface obstructing the extended use of NZVI[26].

The aforementioned issues can be solved by supporting the NZVI surface on different organic or inorganic supports such as starch, chitosan, dextran, silica, biochar, bentonite and kaolinite[27–31]. The introduction of these supports onto the NZVI surface can ameliorate the dispersibility, de-agglomeration, stability, reactivity, and reducibility and avert the oxidation of NZVI surface[32]. On the other hands, several studies for overcoming the drawbacks of Fe^0 have investigated by various methods like doping the surface by nobel metals (e.g.; Cu, Ni, Au and Ag) and coating with $Mg(OH)_2$ overcoming the poor mobility and low suspension stability of bare-Fe^0 [33,34].

Therefore, NZVI was either supported on inorganic silica gel (Si) or organic starch (St) supports to fabricate zero-valent based composite nanomaterial. These composites were evaluated for the adsorption and reduction of Cr(VI) due to the low-cost, high stability and green nature of these stabilizers. Kumari et al. (2020) synthesized NZVI modified with starch for the removal of chromium[31]. The results showed that the removal efficiency of chromium was lower than 50% in the case of pure NZVI compared to nearly 65% using NZVI supported on starch. Furthermore, SEM images confirmed the reduction of nanoparticles aggregation after the modification by starch. Wang et al. (2021) synthesized zero-valent iron coated with silica for the decolorization of acid red 73 dye[35]. Acid red 73 with an initial concentration of 100 mg L^{-1} was completely removed after 120 min using 2 g/L of the silica modified NZVI. Additionally, the performance of NZVI can be improved by adding an oxidizing agent (e.g., H_2O_2) due to its ability to enhance the corrosion of NZVI[36]. Moreover, reactive radicals can be produced via the activation of H_2O_2 by the active sites on the NZVI surface and the reactive species can contribute to the reduction of Cr(VI)[37].

In this study, the optimization of the preparation process of NZVI was conducted. Furthermore, the optimum prepared NZVI based on the production yield and it is affecting on dye decolorization was modified with silica gel or starch and the synthesized nanomaterials were characterized. The performance of the synthesized nanomaterials for the adsorption and chemical reduction of Cr(VI) was studied. Furthermore, the adsorption integrated with the reduction of Cr(VI) by the synthesized materials under different operating parameters such as pH and initial pollutant concentration was investigated. The effects of the co-existence of anions, cations, and natural organic matter on the removal efficiency of Cr(VI) were explored. Additionally, isotherms, thermodynamics, and kinetics of the adsorption process were studied. The reusability performance of the synthesized materials was evaluated, and the removal mechanism was explained. This is the first study to gain better insights into the role of silica supported Fe^0 on the boosting removal of Cr (VI) ions after optimizing the synthetic procedures of Fe^0.

Results and discussion

Optimization of the preparation process of NZVI. The effects of reaction time, reducing agents, and iron precursors on the preparation process of NZVI were optimized based on NZVI yield and the performance of the prepared NZVI towards the decolorization of acid blue-25. The preparation process of NZVI requires a suitable reaction time to obtain metallic iron nanoparticles, so the preparation of NZVI was conducted at reaction times of 10, 30, 60 and 120 min using $NaBH_4$ and $FeCl_2.4H_2O$ as a reducing agent and iron precursor, respectively. The yield of NZVI and removal efficiency of dye decreased with raising the reaction time as shown in Fig. 1a,b, respectively. The NZVI yield decreased from 37.38% to 8.4% by extending the time from 10 to 120 min and the removal efficiency of the dye decreased from 66.7 to 16.5%. The extension of reaction time may increase the tendency of NZVI surface oxidation and the formation of iron oxides. It was noticed that the increase in time resulted in the raising of rusting. So, the optimum reaction time for NZVI production was considered as 10 min.

The reducing agent has a significant role in the preparation process of NZVI. To specify the most proper reducing agent for NZVI synthesis, $NaBH_4$, N_2H_4, NaOH and NH_4OH with 4 M were used as reducing agents following the previously mentioned synthesis procedures of NZVI.

In the case of using $NaBH_4$, a black magnetic precipitate was produced. However, NaOH and N_2H_4 produced a brown precipitate showing lower magnetic properties. In the case of NH_4OH, a non-magnetic green color precipitate was formed. The results showed that N_2H_4, NaOH and NH_4OH could not effectively reduce the iron salt to its zero state. Therefore, $NaBH_4$ was the most suitable reducing agent for the preparation of NZVI.

Four iron salts were used ($FeCl_2.4H_2O$, $FeCl_2$, $FeSO_4.7H_2O$ and $FeCl_3.6H_2O$) to specify the best iron salt for the preparation of NZVI based on the yield (%) and dye removal efficiency (%) as demonstrated in Fig. 1c,d. The preparation process was conducted using the optimum reaction time and reducing agent. The results indicated

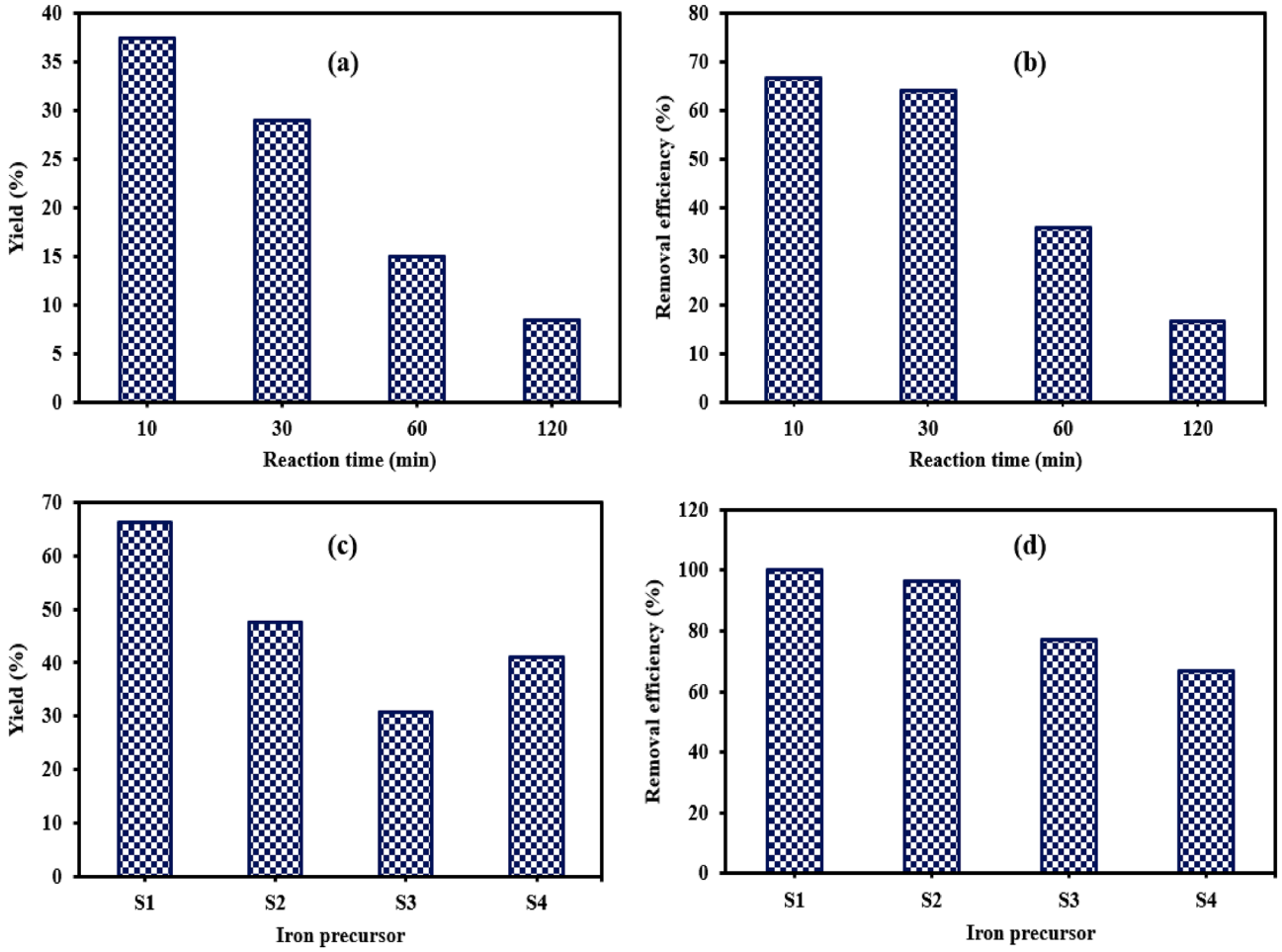

Figure 1. Effect of reaction time on (**a**) NZVI yield (%) and (**b**) removal efficiency of acid blue-25 (%) and Effect of iron salt on (**c**) NZVI yield (%) and (**d**) removal efficiency of acid blue-25 (%). (S1: $FeCl_2.4H_2O$, S2: $FeCl_2$, S3: $FeCl_3.6\ H_2O$, S4: $FeSO_4.7H_2O$, dye concentration = 50 mg L^{-1}, NZVI dose = 0.1 g, solution volume = 100 mL, agitating time = 60 min, agitation rate = 200 rpm).

that $FeCl_2.4H_2O$ attained the highest yield (66.35%) and removal efficiency of dye (99.9%) compared to other salts. Moreover, the results confirmed that the preparation of NZVI by Fe(II) was better than that produced using Fe(III). Therefore, the optimum iron salt for NZVI production was $FeCl_2.4H_2O$.

In the synthesis of NZVI, the economic cost into consideration for the need of the clean water, especially in developing countries. Hence, in the calculations for removal efficiency, it is important to calculate the cost-effectiveness index of the nZVI-synthesis parameters, especially with the optimization of different reducing agents due to the cost of reducing agent is so high. In addition, the relevant cost and energy consumption should be taken into consideration for a practical optimization[38].

Physico-chemical characteristics of the synthesized nanomaterials. TEM image of bare NZVI (Fig. 2a) showed a chain-like agglomeration of nanoparticles, whereas the aggregation of nanoparticles in the case of NZVI-St and NZVI-Si as shown in (Fig. 2b,c) was lower confirming the role of different supports as stabilizers in providing the required repulsive forces between nanoparticles. The nanoparticles had a spherical shape with low tendency of aggregation for the composite materials with a particle size ranged from 20 to 50 nm in the case of pure NZVI and modified NZVI. The grey area in TEM images of NZVI-Si and NZVI-St is attributed to silica gel and starch supporting materials confirming the excellent support of NZVI on silica gel and starch. Moreover, high-resolution TEM images in Fig. 2d–f insured the excellent support of NZVI on silica gel or starch.

To investigate the chemical composition of the synthesized nanomaterials, the EDS pattern in Fig. S1a–c showed the growth of Fe and O in the case of NZVI confirming the partial oxidation of NZVI, whereas the presence of Fe, O and Si in the case of NZVI-Si and Fe, O and C for NZVI-St was affirmed. Moreover, EDS elemental mapping in Fig. 3a–h reconfirmed the chemical composition of the synthesized nanomaterials. Additionally, the EDS and elemental mapping analyses were performed after the removal of Cr(VI) and the results demonstrated the introduction of Cr to the chemical composition in the case of NZVI and NZVI-Si as shown in Fig. 3i–q which insures the adsorption of Cr(VI) on the surface of the adsorbent. SAED patterns in Fig. S2 showed the crystallinity of the synthesized materials.

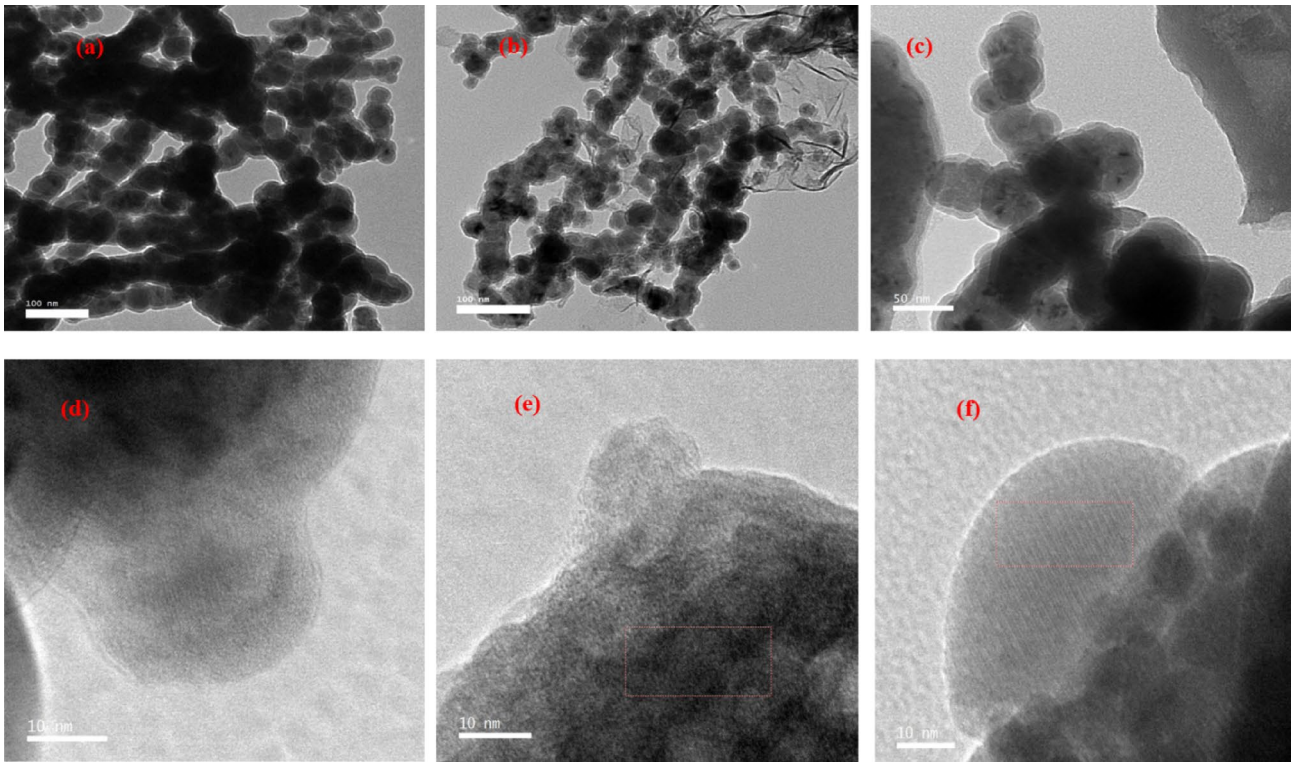

Figure 2. TEM images of (**a**) NZVI, (**b**) NZVI-St and (**c**) NZVI-Si; and high-resolution TEM images (**d**) NZVI, (**e**) NZVI-St and (**f**) NZVI-Si.

Figure 4a show the XRD patterns of NZVI, NZVI-St and NZVI-Si. The significant peak at around 45° is ascribed to the NZVI diffraction plane (110) (JCPDS, file No. 87–0722), whereas there is no peak nearly 35° is imputed to the (311) diffraction plane of Fe_3O_4 , confirming there is no or rare formation of the iron oxide layer on the NZVI surface during the preparation process[39,40]. Chemical structures of the three zero-valent based nanomaterials were confirmed using FTIR analysis. The bands at around 1618 and 3423 cm^{-1} are ascribed to bending and vibration of the O–H bond owing to the adsorbed water molecules on the adsorbent's surface in the case of NZVI, whereas the bands at 3417 and 1635 cm^{-1} in the case of NZVI-Si are ascribed to the presence of O–H bond besides the existence of stretching vibrations of Si–O–Si group at 1095 cm^{-1} as depicted in Fig. 4b [41,42]. Regarding NZVI-St, the band at 2912 cm^{-1} is allocated to the CH_2OH group in the starch which confirms the excellent support of NZVI on starch and the bands at 1624 and 3424 cm^{-1} are imputed to the adsorbed water molecules on the surface[41]. The bands around 1030 cm^{-1} and 1380 cm^{-1} are ascribed to the C-O and COO^- bonds respectively which are presence at NZVI, NZVI-Si and NZVI-St[43]. The bands at nearly 484, 476 and 565 cm^{-1} are allocated to the stretching vibrations of Fe–O in the case of NZVI and its composites NZVI-Si and NZVI-St, respectively[44]. As shown in Fig. 4c, both NZVI and NZVI-St showed type-II adsorption isotherm, while NZVI-Si showed type-IV isotherm. The porous texture of NZVI-Si is different from NZVI and NZV-St, confirming the characteristic effect of the mesoporous structure of silica in NZVI-Si. In addition, NZVI-Si presents a developed few micropore structures that strongly favors high surface area values compared to those for NZVI and NZVI-St. The calculated surface areas of the three prepared materials NZVI, NZVI-St and NZVI-Si were 12, 14, and 60 m^2/g, respectively, confirming the significant enhancement of surface area after the support on silica that resulted to the excellent adsorption performance of NZVI-Si. In Fig. 4d, NZVI-Si has a higher mesopore volume than NZVI-St, resulting in the higher removal of pollutants via pore. The magnetic saturation values (Fig. 4e) were 38.312, 33.44, and 35.756 emu/g, in the case of NZVI, NZVI-St, and NZVI-Si, respectively, which elucidate the ferromagnetic characteristics of the synthesized nanomaterials. However, the reduction of magnetic saturation values in the case of NZVI-St and NZVI-Si was due to the non-magnetic properties of the supporting materials either starch or silica. Although their magnetic characteristics are weaker than those of NZVI, it is stated that samples have outstanding magnetic properties to facilitate separation.

XPS spectra affirmed the presence of Fe and O and Fe, O and Si in the case of NZVI and NZVI-Si, respectively as shown in Fig. 5a. The peaks at nearly 531.40, 531.08 and 533.08 eV are ascribed to O_{1s} in the case of pure NZVI, whereas the peaks at around 531.22, 530.52 and 531.82 eV are attributed to O_{1S} in the case of NZVI-Si[45] as depicted in Fig. 5b,d. The peaks at about 723.68, 710.66 eV and 719.76 eV in Fig. 5c,e are imputed to Fe $2p_{1/2}$, Fe $2p_{3/2}$ and Fe^0, respectively which reconfirms the formation of the iron oxide layer in the case of NZVI and NZVI-Si[46]. The peak at nearly 101.56 eV is ascribed to the Si 2p which affirms the excellent support of NZVI on Si (Fig. 5f)[26].

The existence of the Cr 2p peak revealed that the Cr(VI) was successfully trapped on the NZVI-Si (Fig. 5g). The high resolution XPS spectra were recorded after the Cr(VI) removal process and insignificant shifts in the

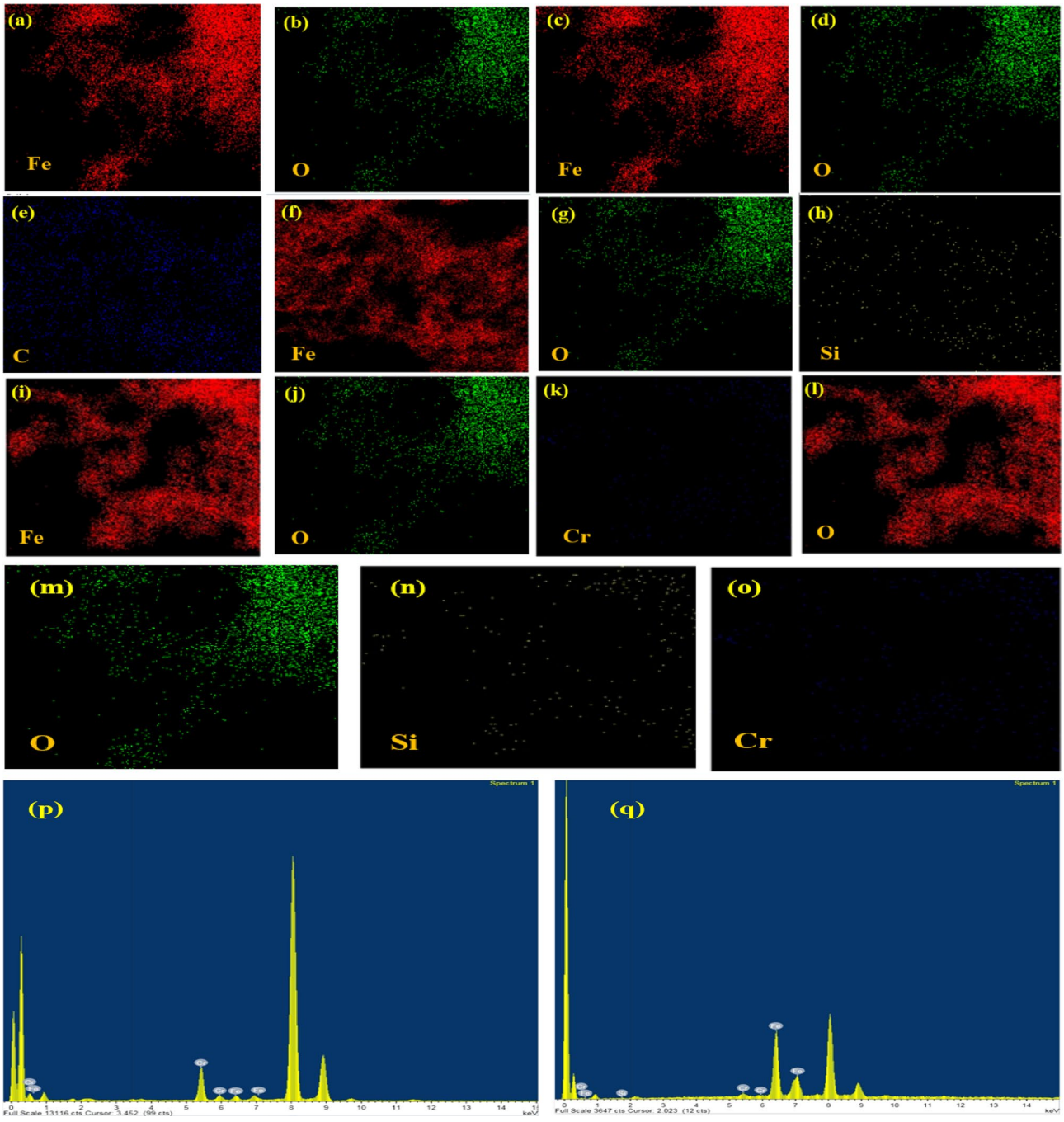

Figure 3. EDX elemental mapping of NZVI (**a**) Fe and (**b**) O; NZVI-St (**c**) Fe, (**d**) O and (**e**) C; NZVI-Si (**f**) Fe, (**g**) O and (**h**) Si; NZVI after Cr(VI) removal (**i**) Fe, (**j**) O and (**k**) Cr; NZVI-Si after Cr(VI) removal (**l**) Fe, (**m**) O, (**n**) Si and (**o**) Cr and EDS pattern after Cr(VI) removal of (**p**) NZVI and (**q**) NZVI-Si.

binding energies were observed due to the complexation between Cr(VI) and the adsorbents' surface as shown in Fig. 5g–m. The peak at 581.9 eV is ascribed to Cr(VI) which affirms the adsorption of Cr(VI) on the surface (Fig. 5n). Additionally, the peaks at 577.68 and 588.23 eV are attributed to Cr $2p_{3/2}$ and Cr $2p_{1/2}$ of Cr(III), respectively in the case of NZVI and confirming the reduction of Cr(VI) to Cr(III) after adsorption on the materials surfaces[40]. The existence of Fe^0 peak after Cr(VI) removal suggests the high reusability capability of both NZVI-Si and NZVI-St.

Effect of pH and initial Cr(VI) concentration on the removal performance. Figure 6a portrays the effect of pH on the removal efficiency of Cr(VI) and the adsorption capacity of the synthesized nanomaterials at an adsorbent dose of 0.1 g/100 mL, initial Cr(VI) concentration of 10 mg L^{-1}, contact time of 120 min and temperature of 20 °C. The removal efficiencies decreased from 91.9 to 49%, 96 to 51.8% and 98 to 54.5% by raising the pH from 1 to 11 using NZVI, NZVI-St and NZVI-Si, respectively. Kumari et al. (2020) reported the

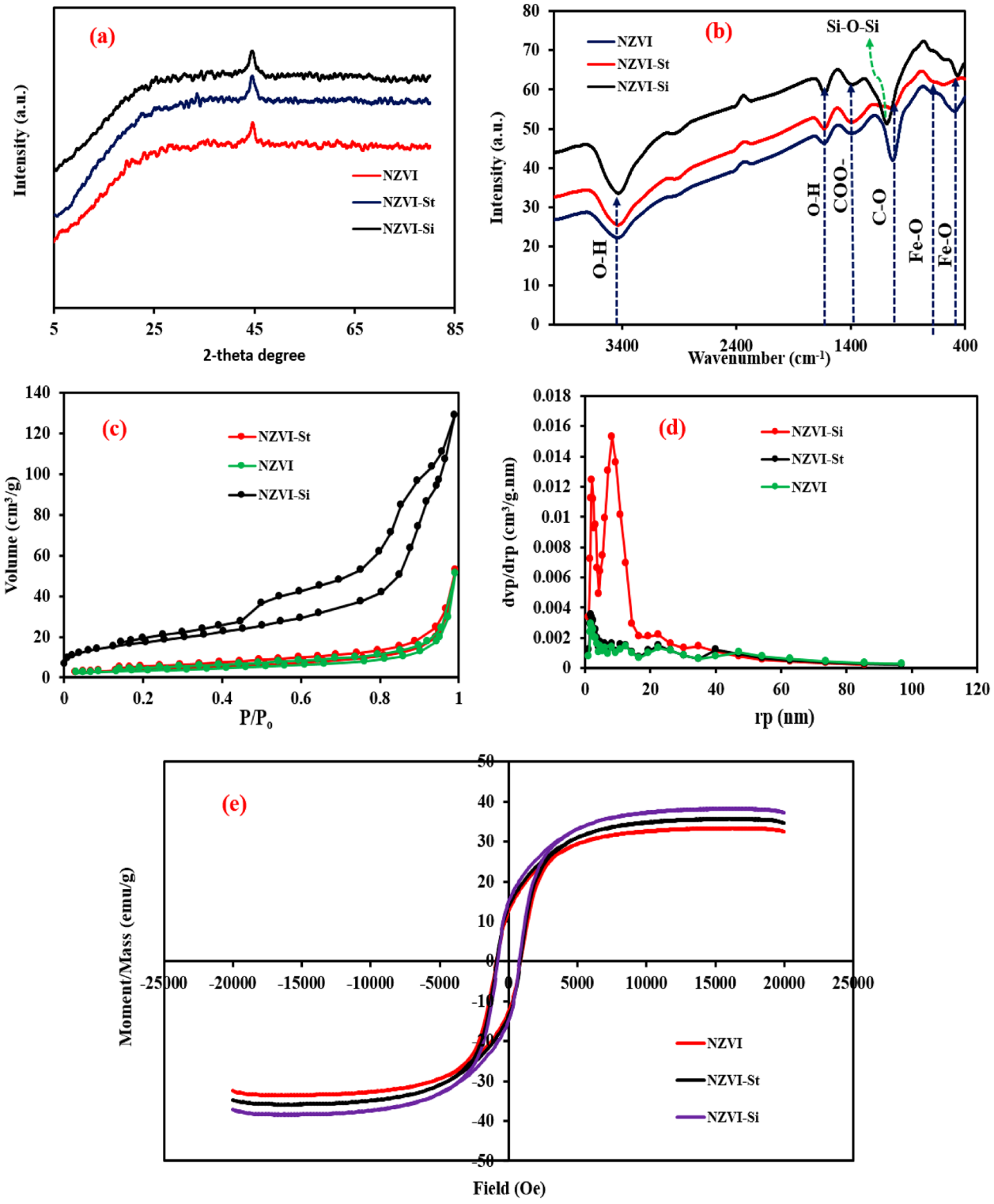

Figure 4. (**a**) XRD patterns; (**b**) FTIR spectra; (**c**) adsorption–desorption isotherms; (**d**) pore size distribution and (**e**) VSM of NZVI, NZVI-St and NZVI-Si.

improvement of Cr(VI) removal at low pH value using starch modified NZVI[33]. At low pH values (1-3), NZVI and modified NZVI showed high removal performance and adsorption capacity. The synthesized nanomaterials can be easily corroded at low pH values which contributes to the dissolution of Fe^0 and the production of hydrogen and Fe^{2+} (secondary reductants) as shown in Eqs. (1,2)[4,47]. Moreover, low pH values can participate in the dissolution of the passivation layer formed on the NZVI surface which provides fresh active sites[48]. The point of zero charge (PZC) of NZVI, NZVI-Si and NZVI-St were estimated to be 7.2, 8.1 and 7.8, respectively. At a pH value lower than the PZC, the adsorbents' surface charge becomes positive. Therefore, the removal efficiency

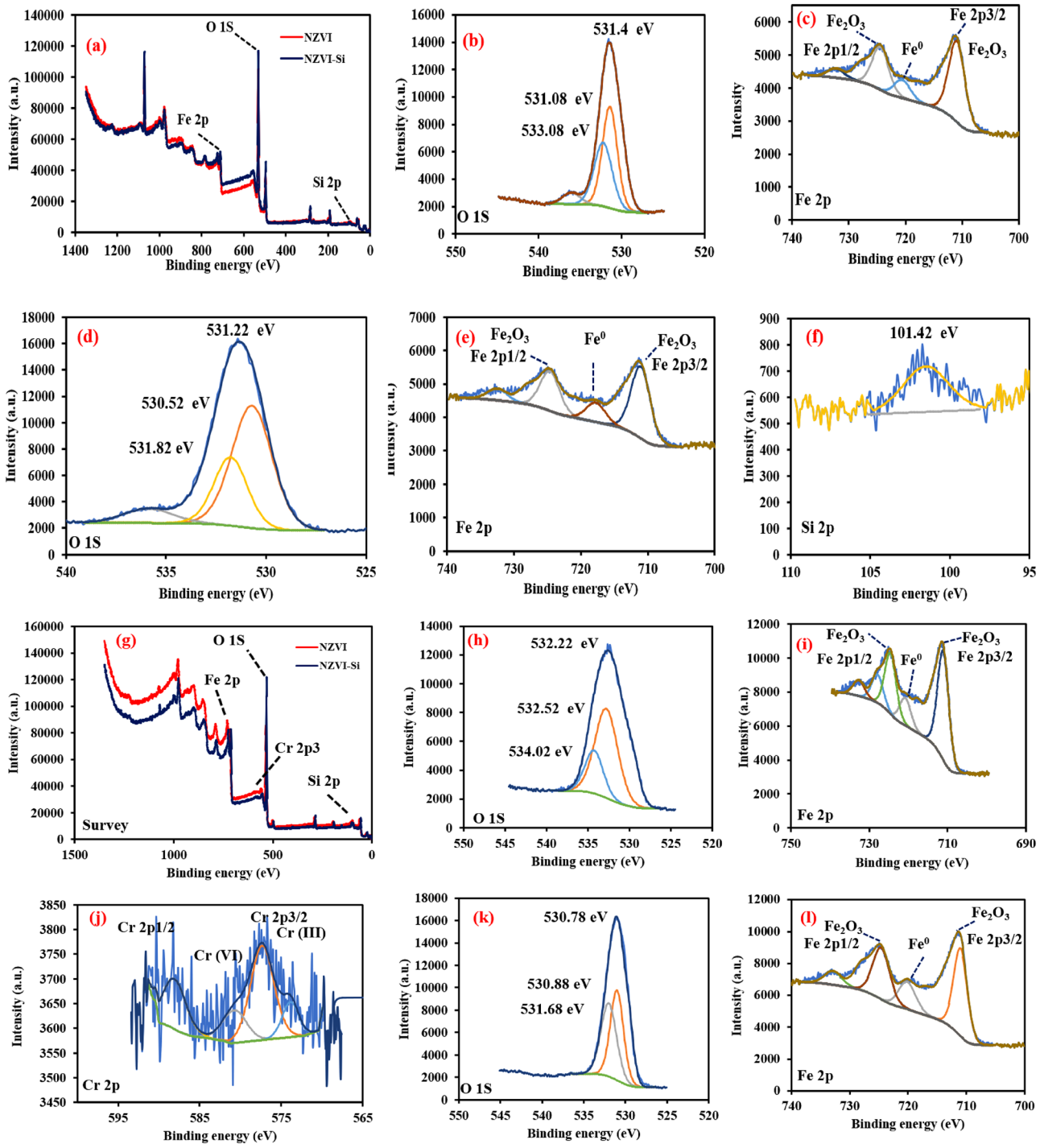

Figure 5. (**a**) XPS survey of NZVI and NZVI-Si, (**b**) O $_{1s}$ spectra and (**c**) Fe $_{2p}$ spectra of NZVI, (**d**) O $_{1s}$ spectra, (**e**) Fe $_{2p}$ spectra and (**f**) Si $_{2p}$ spectra of NZVI-Si, (**g**) XPS survey of NZVI and NZVI-Si after Cr(VI) removal, (**h**) O $_{1s}$ spectra, (**i**) Fe $_{2p}$ spectra and (**j**) Cr $_{2p}$ spectra of NZVI, (**k**) O $_{1s}$ spectra, (**l**) Fe $_{2p}$ spectra, (**m**) Si $_{2p}$ and (**n**) Cr $_{2p}$ of NZVI-Si.

was enhanced due to the attractive forces between positively charged NZVI, NZVI-Si and NZVI-St and Cr(VI) anions, because Cr(VI) exists in the form of $HCrO_4^-$ and CrO_4^{2-} over a wide pH range[47].

The increase in pH decreased the removal efficiency of Cr(VI) and the adsorption capacity of NZVI, NZVI-St and NZVI-Si because of the repulsive forces between NZVI, NZVI-Si and NZVI-St and Cr(VI) anions[4]. Furthermore, iron hydroxides can be easily formed on the adsorbents' surface in alkaline conditions, and they can block the active sites which decreases the reactivity of NZVI, NZVI-Si and NZVI-St[48]. Moreover, the iron oxides on the adsorbents' surface can de-accelerate the electron transfer from the adsorbent to sorbent[49]. The removal efficiency was enhanced in alkaline conditions using modified NZVI, as silanol groups in the support can be separated and provide protons that maintain the pH and prevents the passivation[4].

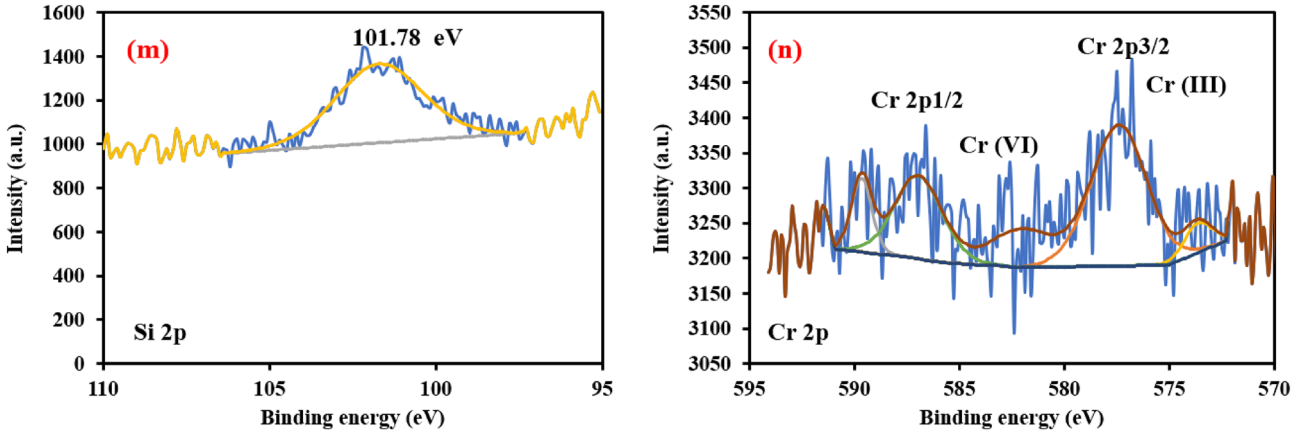

Figure 5. (continued)

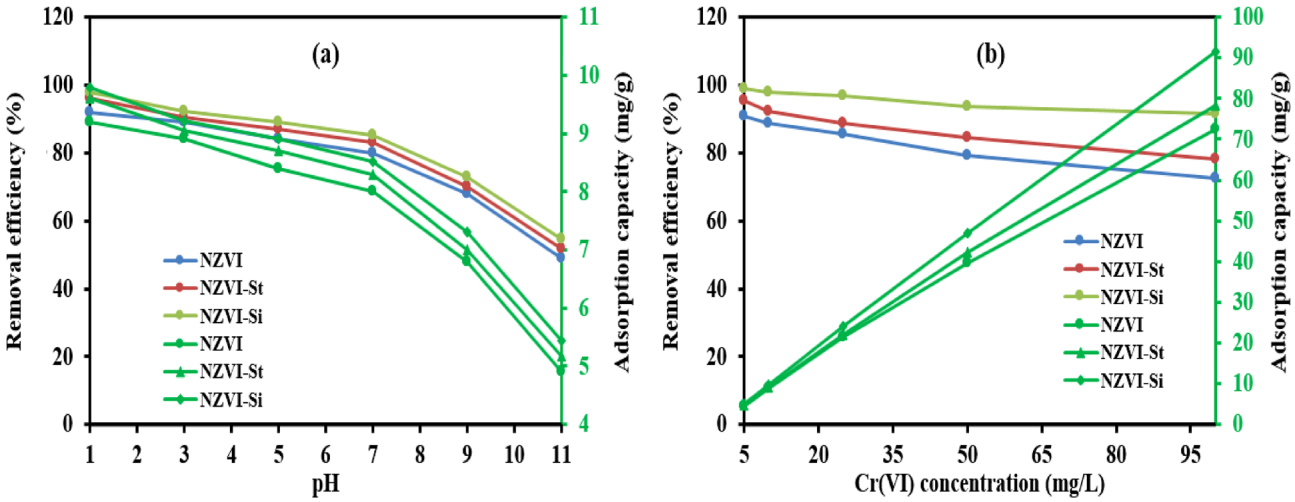

Figure 6. (**a**) Effect of pH and (**b**) Effect of initial Cr(VI) on the removal efficiency of Cr(VI) and adsorption capacity of synthesized materials.

Figure 6b shows the effect of initial Cr(VI) concentration on the adsorption capacity of NZVI, NZVI-Si and NZVI-St and the removal efficiency of Cr(VI). NZVI-Si and NZVI-St showed higher removal performance compared to pristine NZVI at different initial Cr(VI) concentrations due to the reduction of aggregation of nanoparticles after the support on silica and starch as explained in the characterizations section. Moreover, the introduction of these supports can reduce the oxidation of the adsorbents' surface and inhibit the formation of passivation layer which facilitates the electron transfer between NZVI and Cr(VI). Also, the amelioration of the removal performance of Cr(VI) in the case of modified NZVI was due to the increase in the surface area.

The increase of adsorption capacity from 4.95 to 91.5 mg g^{-1} by raising the initial concentration of Cr(VI) from 5 to 100 mg L^{-1} at pH 1, contact time of 120 min, the temperature of 20 °C and NZVI-Si dose of 0.1 g/100 mL was owing to the ameliorated driving forces between Cr(VI) and reactive sites. On the other hand, the removal efficiency of Cr(VI) went down from 90.8 to 72.4%, 95.6 to 78.3% and 99 to 91.5%, respectively with the increase of initial Cr(VI) concentration from 5 to 100 mg L^{-1} using NZVI, NZVI-St and NZVI-Si, respectively. In the case of low concentrations of Cr(VI), the active sites on the NZVI, NZVI-Si and NZVI-St are adequate for the reduction and adsorption of Cr(VI). However, in the case of high concentrations of Cr(VI), the reactive sites are not enough to adsorb the high number of Cr(VI) ions which inhibits the appropriate contact between the adsorbents and Cr(VI) ions[50]. Moreover, the formation of passivation layer on the adsorbents' surface can be accelerated in the case of high Cr(VI) concentration which reduces the reactivity of the synthesized adsorbents with Cr(VI) and prevents the electron transfer from NZVI surface to Cr(VI)[51,52]. Zhou et al. (2022) reported the same trend during the removal of Cr(VI) by a modified NZVI[53]. Due to the superiority of NZVI-Si for Cr(VI) adsorption is over NZVI-St and NZVI, NZVI-Si. It was selected to investigate the remaining parameters affected on Cr(VI) removal as well as the experimental data of Cr(VI) removal using NZVI-Si were fitted using adsorption kinetic, isotherm and thermodynamic models.

$$2HCrO_4^- + 3Fe^0 + 14\,H^+ \rightarrow 2\,Cr(III) + 3\,Fe(II) + 8\,H_2O \quad (1)$$

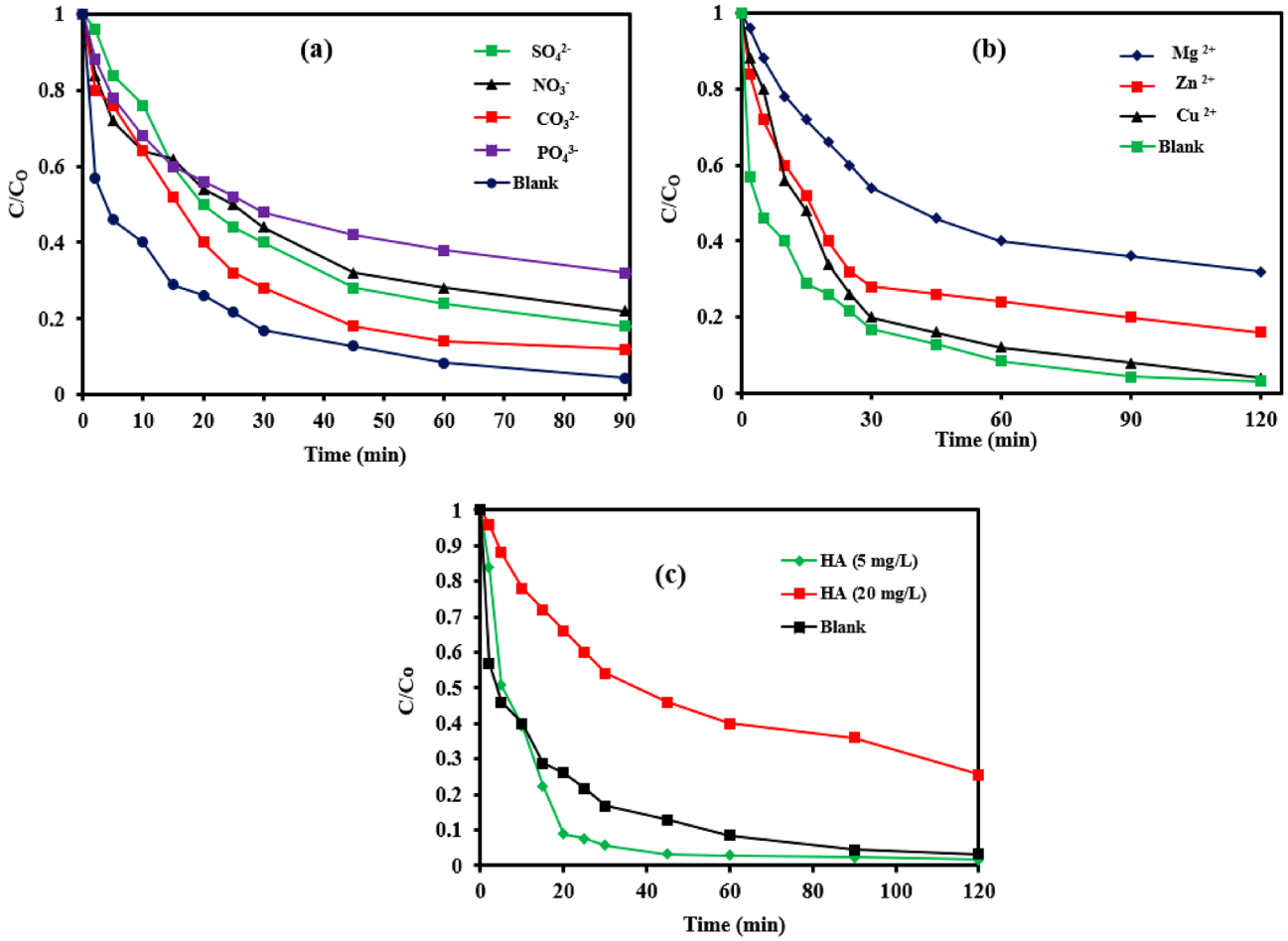

Figure 7. (**a**) Effect of co-existing (**a**) anions, (**b**) cations and (**c**) humic acid on the removal efficiency of Cr(VI) by NZVI-Si.

$$HCrO_4^- + 3\,Fe(II) + 7\,H^+ \rightarrow Cr(III) + 3\,Fe(III) + 4\,H_2O \quad (2)$$

Effect of co-existing cations, anions and humic acid on the removal efficiency. The influences of the presence of anions, cations and natural organic matter such as humic acid (HA) on the Cr(VI) removal efficiency onto NZVI-Si were explored to simulate the real application, as real wastewater contains a mixtures of species such as inorganic ions and natural organic matter. Fig. 7a shows the effect of the presence of anions (e.g., NO_3^-, CO_3^{2-}, SO_4^{2-}, PO_4^{3-}) with a concentration of 40 mg L^{-1} on the removal efficiency of Cr(VI). The removal efficiencies of Cr(VI) were 83.6%, 79.6%, 90.2% and 75.6% after adding SO_4^{2-}, NO_3^-, CO_3^{2-} and PO_4^{3-}, respectively compared to 96.8% in the case of no anions at NZVI-Si dose of 0.1 g/100 mL, initial Cr(VI) concentration of 25 mg L^{-1}, contact time of 120 min and temperature of 20 °C. In spite of the improvement of the ionic strength after adding the aforementioned anions, they can compete with Cr(VI) and occupy the binding sites which de-accelerate the removal of Cr(VI)[53]. Furthermore, anions such as CO_3^{2-} and PO_4^{3-} can form inner-sphere complexes with iron (oxy) hydroxides and the formed complexes can block the active sites reducing the removal efficiency[54].

The investigation of the influence of the existence of cations such as Mg^{2+}, Zn^{2+} and Cu^{2+}on the removal efficiency of Cr(VI) was carried out as shown in Fig. 7b at NZVI-Si dose of 0.1 g/100 mL, initial Cr(VI) concentration of 25 mg L^{-1}, contact time of 120 min, cations concentrations of 40 mg L^{-1} and temperature of 20 °C. The removal efficacy of Cr(VI) was 96.8% in the case of no-cations, whereas the addition of Mg^{2+} and Zn^{2+} decreased the removal efficiencies to 68% and 84%, respectively. Mg^{2+} and Zn^{2+} ions can occupy the reactive sites instead of Cr(VI) which decreases the removal efficiency of Cr(VI). On the other hand, the removal efficiency of Cr(VI) was 96% after adding Cu^{2+}. The electron transfer and corrosion of Fe^0 can be improved owing to the formed bimetallic surface after adding Cu^{2+}. The enhancement of electron transfer and corrosion after the addition of Cu^{2+} can overweigh the negative effect of the occupation of binding sites by Cu^{2+} ions leading to high removal efficiency approximately the same as the blank sample. Chen et al. (2016) stated the improvement of the removal of hexachlorobenzene after Cu^{2+} addition using NZVI composited with activated carbon[54].

The removal efficiency of Cr(VI) was enhanced to 98.4% in the presence of 5 mg L^{-1} of HA compared to 96.8% in the absence of HA as shown in Fig. 7c at NZVI-Si dose of 0.1 g/100 mL, initial Cr(VI) concentration

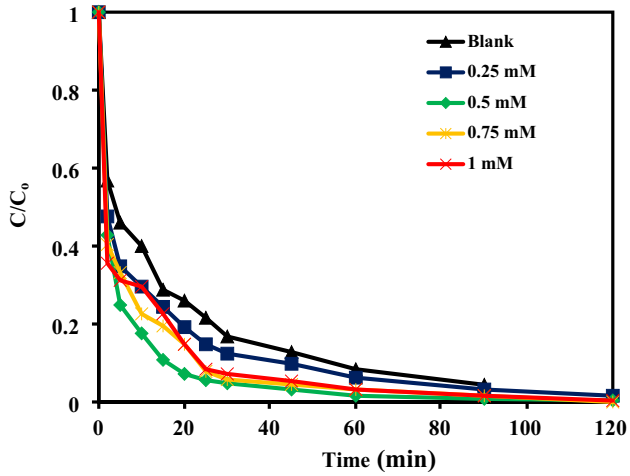

Figure 8. (**a**) Effect of the addition of different concentrations of H_2O_2 on the removal efficiency of Cr(VI) at NZVI-Si dose of 0.1 g/100 mL, initial Cr(VI) concentration of 25 mg/L, contact time of 120 min, and temperature of 20 °C.

of 25 mg L^{-1}, contact time of 120 min, and temperature of 20 °C. The presence of humic acid can propel the removal of Cr(VI) due to its ability to act as an electron shuttle enhancing the electron transfer between NZVI and Cr(VI)[51]. Moreover, the formation of NOM agglomeration on the NZVI-Si surface can ameliorate the adsorption of Cr(VI) on the NZVI-Si surface. Lv et al. (2013) reported an increase in the Cr(VI) removal efficiency after adding 5 mg L^{-1} of HA[55]. The raising of HA concentration to 20 mg L^{-1} decreased the removal efficiency of Cr(VI) to 74.4%. At high concentrations of humic acid, it can compete with Cr(VI) for the adsorption on the NZVI-Si surface. Moreover, HA can react with (Fe^{2+}/Fe^{3+}) decreasing the number of binding sites. Beside complexes may be formed between humic acid and iron ions which inhibit the formation of corrosion products involved in the removal of Cr(VI)[36].

Effect of the addition of H_2O_2 on the removal of Cr(VI) by NZVI-Si. The addition of 0.25, 0.5 and 0.75 mM of H_2O_2 to the adsorption system ramped the removal efficiency to 98.4, 99.6% and 100%, respectively, whereas it was 96.8% without adding H_2O_2 as shown in Fig. 8. The generated radicals after the activation of H_2O_2 by NZVI-Si can produce reducing conditions that can contribute to the reduction of Cr(VI) to Cr(III). Moreover, the introduction of H_2O_2 can speed up the corrosion of NZVI-Si[36]. The increase of H_2O_2 concentration can support the generation of more radicals, accelerate the NZVI-Si corrosion, and the reduction of Cr(VI)[36]. However, the increase of H_2O_2 to 1 mM decreased the removal efficiency due to its scavenging impact towards generated radicals at elevated concentrations[37]. Moreover, the reduced Cr(III) can be reconverted to Cr(VI) at high H_2O_2 concentrations[36].

Adsorption kinetics. The pseudo-first-order rate constant and coefficient of determination (R^2) were estimated via the linear plot of ln (q_e-q_t) versus time (t) as shown in Fig. 9a. The R^2 was high (0.97); however, there was a significant difference between experimental q_e (23.39 mg g^{-1}) and obtained q_e (18.04 mg g^{-1}) from the pseudo-first-order model. Therefore, the pseudo-first-order model was not efficient to describe the adsorption of Cr(VI) on the NZVI-Si surface. Regarding the pseudo-second-order model, the model constants were estimated from the slope and the intercept of the linear relation between t/q_t and t as depicted in Fig. 9b. The significance of the pseudo-second-order model was affirmed by the high R^2 (0.9972) and the slight difference between experimental q_e (23.39 mg g^{-1}) and calculated q_e (26.8 mg g^{-1}) from the model. The intraparticle diffusion model constants and R^2 were estimated by the linear plot of q_t versus $t^{0.5}$. The multi-linearity in Fig. 9c indicated that the adsorption process took place in three stages as well as the multistage sorption of Cr(VI) on the NZVI-Si surface. The first stage describes the transfer of Cr(VI) from the solution to NZVI-Si outer surface or boundary layer diffusion. The second stage represents the entrance of Cr(VI) ions into the pores by intraparticle diffusion. The third stage refers to the diffusion of Cr(VI) into the small pores till reaching the equilibrium. The lines in Fig. 9c did not pass through the origin affirming that the adsorption of Cr(VI) could be attained via intraparticle diffusion but it was not the only rate-governing step[56]. Moreover, the non-zero intercept in the case of the Boyd model in Fig. 9d reaffirmed that the rate of adsorption was controlled by intraparticle diffusion. The high R^2 of the parabolic diffusion model affirmed that the adsorption of Cr(VI) could occur by intraparticle diffusion as shown in Fig. 9e. Linear plot of q_t versus ln(t) as depicted in Fig. 9f was used to estimate the Elovich model constants and R^2. The high R^2 indicated that Elovich model was satisfactory to describe the adsorption process. Power kinetic model constants were determined via the linear plot of ln(q_t) versus ln(t) and the modest R^2 value expressed that this model could not effectively describe the adsorption process (Fig. 9g). Table 1 shows the kinetic models' constants and R^2.

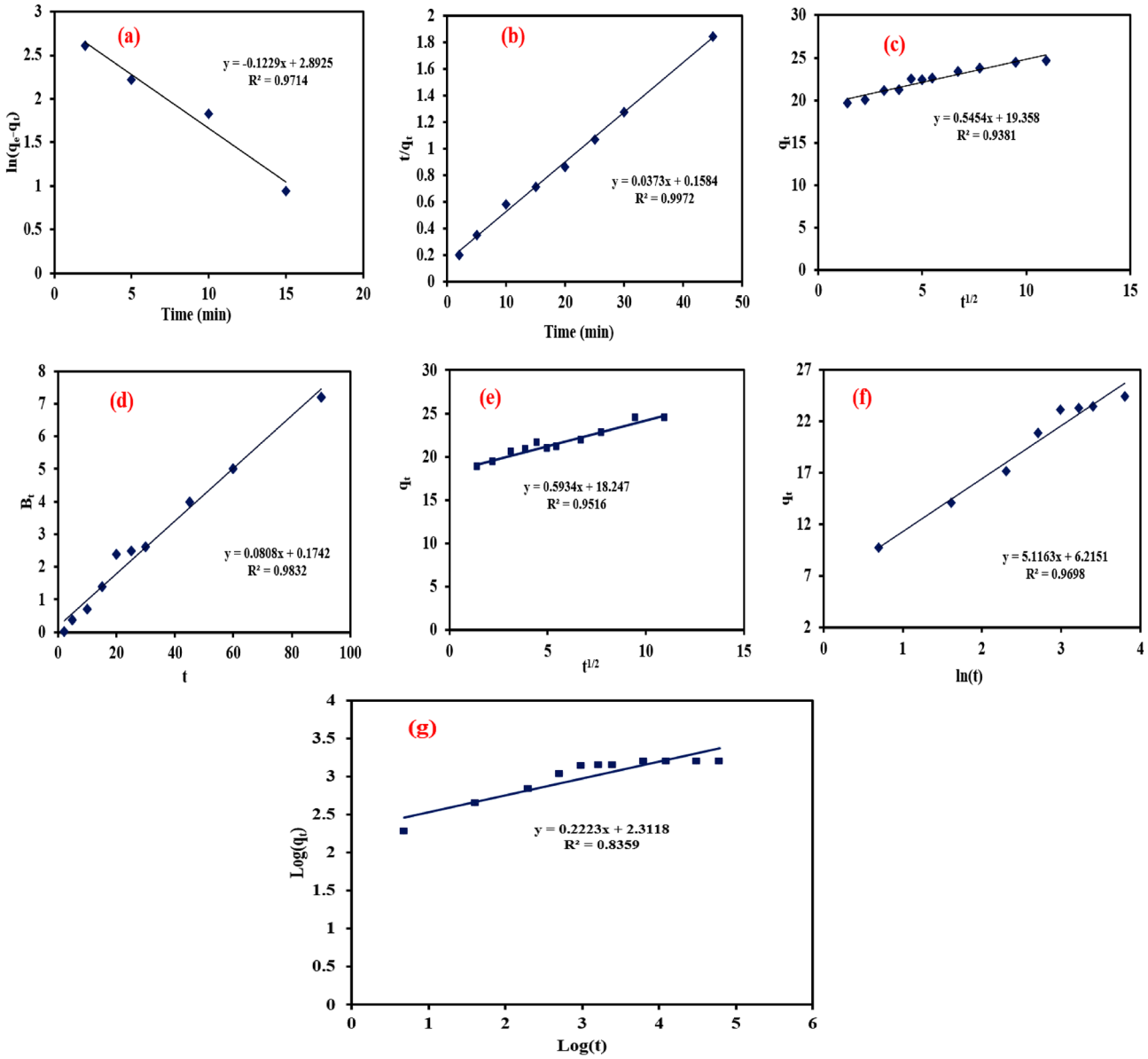

Figure 9. Adsorption kinetics of Cr(VI) (**a**) first-order model, (**b**) second-order model, (**c**) intraparticle diffusion, (**d**) Boyd model, (**e**) parabolic diffusion model, (**f**) Elovich model and (**g**) power function model.

Adsorption isotherms. The linear relation between C_e and C_e/q_e was plotted to estimate the Langmuir isotherm constants and R^2 as portrayed in Fig. 10a. The high R^2 (0.9976) indicated that the adsorption isotherm of Cr(VI) on the adsorbent's surface could be expressed by the Langmuir model. The maximum monolayer adsorption capacity was 149.25 mg g^{-1}. R_L value was lower than 1 confirming the favorable adsorption of Cr(VI) on NZVI-Si surface confirming the suggested mechanism for Cr(VI) removal. Moreover, Freundlich and Temkin isotherm models' constants were estimated from the slope and intercept of the linear plots shown in Fig. 10b,c. The parameters of the different studied equilibrium isotherm models are listed in Table 2. The R^2 was lower in the case of Freundlich and Temkin indicating that Langmuir was more suitable to fit the experimental data. The value of 1/n in Freundlich equation was lower than 1 suggesting the favorability of the adsorption of Cr(VI) on the NZVI-Si surface. The linear plot of ε^2 versus $\ln(q_e)$ could be employed to estimate Dubinin-Radushkevish constants (Fig. 10d). The mean adsorption energy calculated as 17.5 kJ mol^{-1} indicating that the adsorption of Cr(VI) on NZVI-Si surface is physico-chemical adsorption. The low R^2 in the Hankins-Jura model is as shown in Fig. 10e depicted that the adsorption process was monolayer which was in agreement with the results obtained from Langmuir model. The Generalized isotherm model constants were estimated via the linear plot of $\ln(\frac{q_m}{q_e} - 1)$ versus $\ln(C_e)$. The generalized isotherm model could not describe the adsorption process of Cr(VI) on NZVI-Si because of its low R^2 compared to other isotherm models (Fig. 10f).

Kinetic models	Parameters
First-order model	$K_1 = 0.1222\ min^{-1}$ $q_e = 18.04\ mg\ g^{-1}$ $R^2 = 0.9714$
Second-order model	$K_2 = 0.0088\ g\ mg^{-1}\ min^{-1}$ $q_e = 24.8\ mg\ g^{-1}$ $R^2 = .9972$
Elovich model	$\alpha = 17.23\ mg\ g^{-1}\ min^{-1}$ $\beta = 0.195\ g\ mg^{-1}$ $R^2 = 0.9698$
Intraparticle diffusion model	$K_d = 0.5454\ mg\ g^{-1}\ min^{-0.5}$ $C = 19.358\ mg\ g^{-1}$ $R^2 = 0.9381$
Boyd model	$R^2 = 0.9832$
Parabolic diffusion model	$K_p = 0.5934\ (mg\ kg^{-1})^{-0.5}$ $a = 18.247\ mg\ g^{-1}$ $R^2 = 0.9516$
Power function model	$a = 205$ $b = 0.222$ $R^2 = 0.8359$

Table 1. Constants and coefficients of determination of pseudo-first-order, pseudo-second-order, Elovich, Boyd, parabolic diffusion and power function kinetic models.

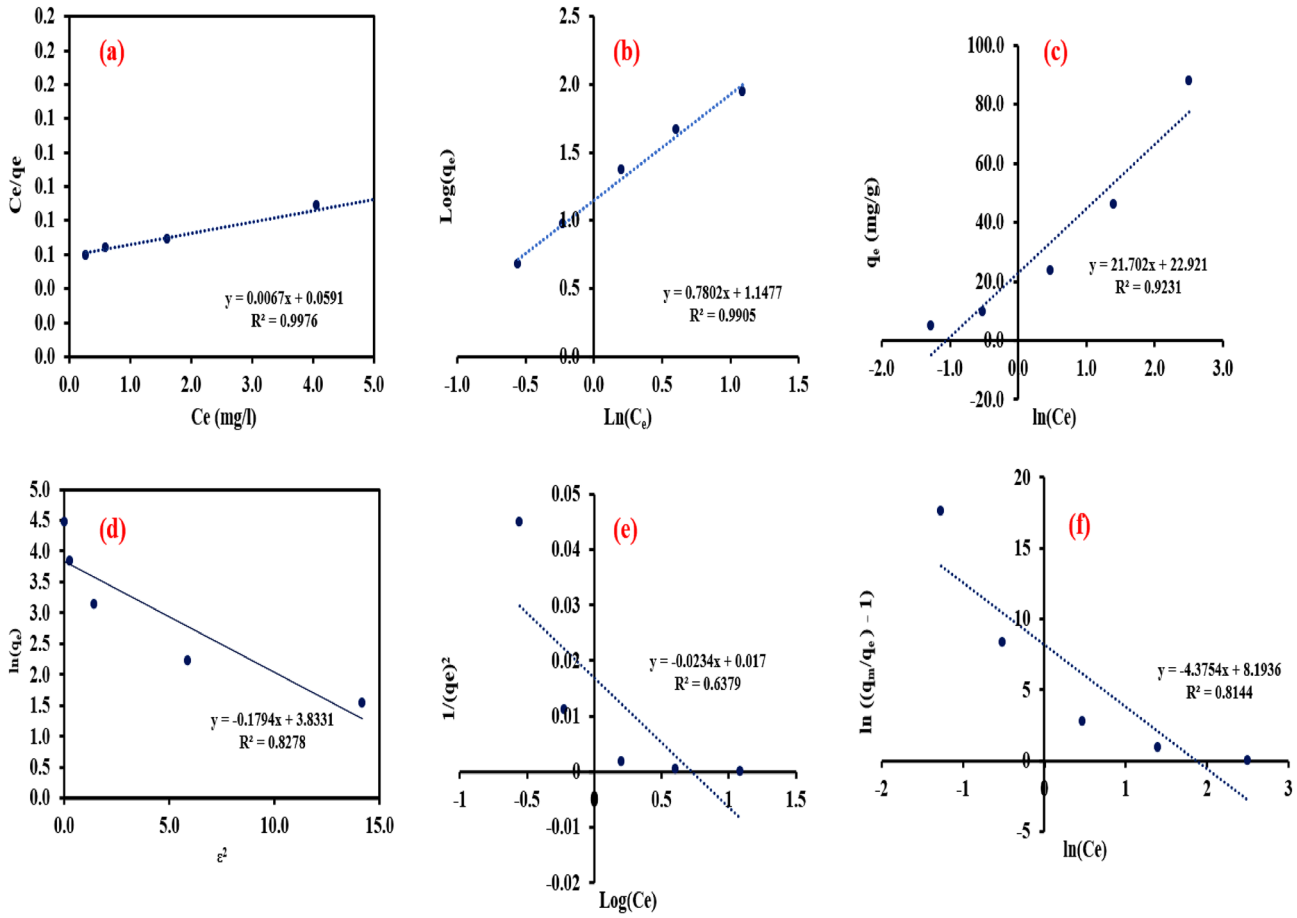

Figure 10. Adsorption isotherms (**a**) Langmuir model, (**b**) Freundlich model, (**c**) Temkin model, (**d**) Dubinin-Radushkevish model, (**e**) Harkins–Jura model and (**f**) Generalized isotherm model.

Adsorption thermodynamics. The linear plot of $\ln(q_e/q_c)$ versus 1/T is shown in Fig. 11. ΔH^o, ΔS^o and ΔG^o values were estimated and listed in Table 3. The negative value of ΔG^o and negative value of ΔH^o suggested the spontaneous and exothermic nature of Cr(VI) adsorption on the NZVI-Si surface. Moreover, the positive value of ΔS^o indicated that the randomness at the sorbent/solution interface was high. The increase of ΔG^o with raising the temperature reflected the increase of spontaneity of the adsorption process with temperature.

Isotherm models	Parameters
Langmuir model	$q_m = 149.25$ mg g^{-1} $K_L = 0.113$ L mg^{-1} $R^2 = 0.9976$ $R_L = 0.0815$
Freundlich model	$K_f = 3.151$ L mg^{-1} $1/n = 0.78$ $R^2 = 0.99$
Temkin model	$b_t = 112.875$ J mol^{-1} $k_t = 2.875$ L mg^{-1} $B = 112.3$ $R^2 = 0.9231$
Dubinin-Radushevish model	$Qs = 44.4$ mg g^{-1} $B = 0.1635$ mol^2 J^{-2} $R^2 = 0.9667$ $E = 17.5$ kJ mol^{-1}
Harkins–Jura model	$A = 42.7$ $B = 0.73$ $R^2 = 0.6379$
Generalized isotherm model	$K = 3617.7$ $N_b = 4.3754$ $R^2 = 0.8144$

Table 2. Constants and coefficients of determination of isotherm models.

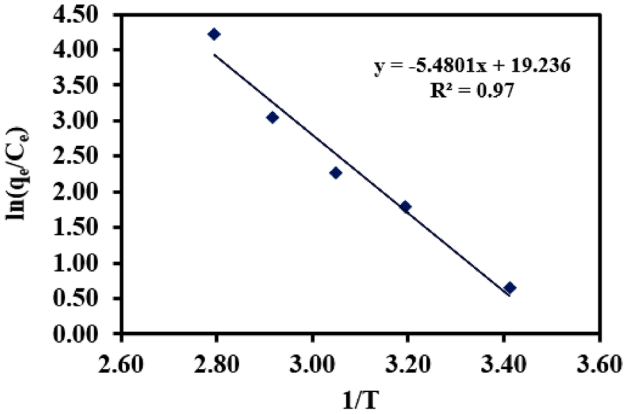

Figure 11. Linear plot of $\ln(q_e/C_e)$ versus 1/T.

Temperature (K)	ΔG^o (KJ mol^{-1})	ΔH^o (KJ mol^{-1})	ΔS^o (J mol^{-1} K^{-1})
293	-1.3	-45.56	159.93
313	-4.5		
328	-6.9		
343	-9.3		
358	-11.69		

Table 3. Parameters of thermodynamic study.

Reusability of NZVI/Si. NZVI-Si was used in repetitive cycles to investigate its reusability performance as shown in Fig. 12. The NZVI-Si particles were collected after each cycle by a magnet, washed with water and dried before the subsequent use. The removal efficiencies were 96.8%, 93.67%, 90.1%, 86.7, 82.9% and 74.8% in the six consecutive runs, respectively. The results indicated the efficient reusability of NZVI-Si. The removal efficiency was higher in the first cycle owing to the availability of active sites. However, the number of binding sites decreased in the following runs. Moreover, the removal efficiency decreased in successive cycles due to the oxidation of NZVI-Si and the formation of a passivation layer in successive cycles[8].

Removal mechanism of Cr(VI) by NZVI-Si. Figure 13 shows the three-step removal mechanism of Cr(VI) (adsorption, reduction and precipitation). NZVI nanoparticles consist of a core and shell. The shell is composed of iron oxides that can be formed via the environmental oxidation of NZVI[51]. Moreover, NZVI can

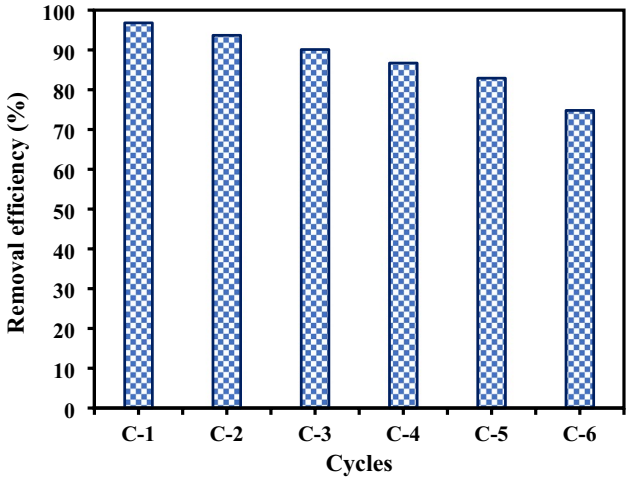

Figure 12. Reusability performance of NZVI-Si at NZVI-Si dose of 0.1 g/100 mL, initial Cr(VI) concentration of 25 mg/L, contact time of 120 min, and temperature of 20 °C.

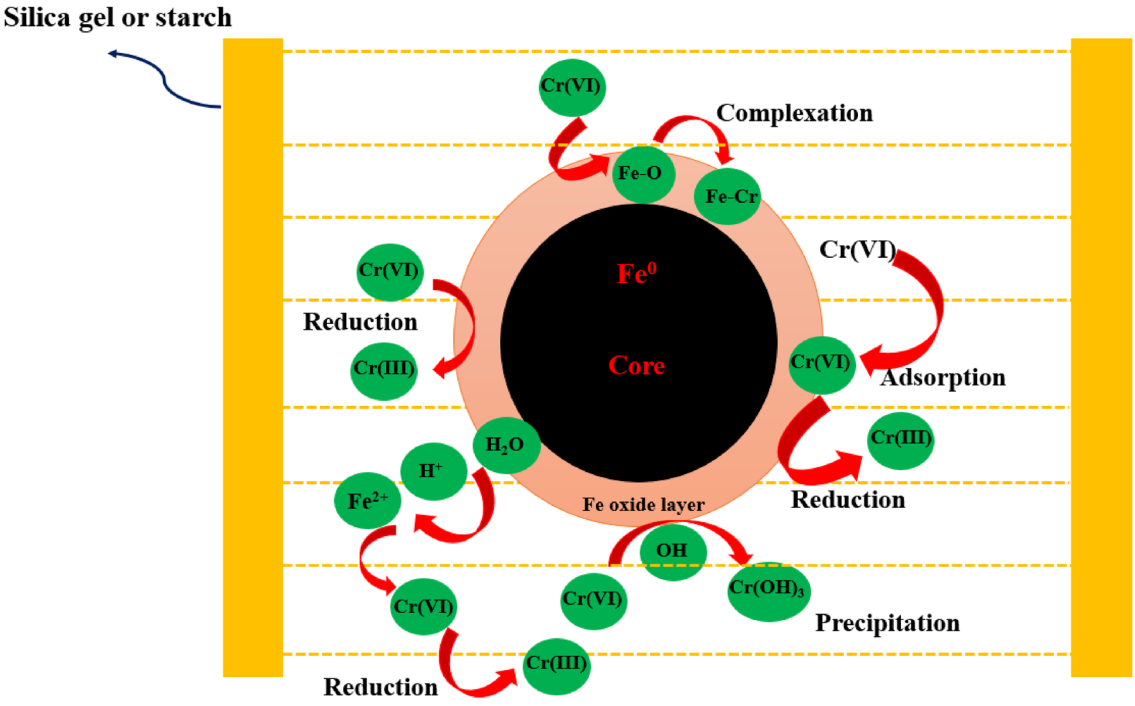

Figure 13. Removal mechanism of Cr(VI) by supported-NZVI.

react with water and oxygen in aqueous solutions forming iron hydroxide layer on the NZVI surface[57]. Cr(VI) can be adsorbed on the NZVI surface, as Cr(VI) can form chemical complexes with iron oxide/hydroxide in the outer layer[58]. The NZVI can react with H_2O generating Fe^{2+} and H^+ (secondary reductants) as given in Eq. (3). Moreover, the iron oxide/hydroxide layer has a high reducing ability that can reduce the adsorbed Cr(VI) to Cr(III)[59]. Then, the $Cr(OH)_3$ can be formed on the NZVI surface and then precipitated as shown in Eq. (4). Moreover, Cr^{3+} can be incorporated into the iron oxide/hydroxide layer forming Fe^{3+}-Cr^{3+} complexes. The formed Fe^{3+}-Cr^{3+} hydroxides can de-accelerate the electron transfer from the core to the surface which inhibits the reduction of Cr(VI) and reduces the removal performance especially at high initial Cr(VI) concentrations[59]. The adsorption of Cr(VI) on NZVI surface was confirmed by EDS, EDS elemental mapping and XPS. Moreover, XPS analysis affirmed the reduction of Cr(VI) to Cr(III).

The support on silica or starch can facilitate the electron transfer and inhibit the rapid oxidation of NZVI surface which improves the removal of Cr(VI)[50]. Moreover, supporting on silica or starch can decrease the agglomeration of NZVI which improves the reactivity, reducibility and dispersibility of NZVI as shown in TEM images. Further, the Cr(VI) can diffuse into the pores of the supporting materials as well as supporting materials can provide NZVI with higher surface area and active sites which increased the adsorption and reduction

performance of bare NZVI[56]. Additionally, the starch or silica can employ as nanoreactors for accelerating the reaction between supported-NZVI and Cr(VI) and the NZVI in the pores can effectively reduce Cr(VI)[60]. The difference between Cr(VI) concentration in the outer and inner pores creates a driving force that participates in attaining frequent adsorption and diffusion of Cr(VI) into the pores till reaching the equilibrium[61]. Thus, the supported-NZVI can effectively remove Cr(VI).

$$Fe^0 + 2\,H_2O \rightarrow Fe^{2+} + H_2 + 2\,OH^- \quad (3)$$

$$2\,Fe^0 + Cr_2O_7^{2-} + 8\,H^+ \rightarrow 3\,Fe^{2+} + 2\,Cr(OH)_3 + H_2O \quad (4)$$

Role of silica in the removal of Cr (VI). From the abovementioned data, the silica supported Fe^0 is faster than that of pure Fe^0. This may be one of three mechanisms which are (i) adsorptive behavior of silica on the surface of Fe^0; (ii) silica as a governer of formation of Fe^0 and possessed a tail-loop surface. Cr(VI) is diffused into the position of tail-loop layers and the availability of Cr(VI) on the surface of Fe^0 would be increased; and (iii) Protection of Fe^0 by silica to provide more contact area of Cr(VI) as a target pollutants.

Materials and methods

Materials. Ferrous chloride ($FeCl_2$, 99%), ferrous chloride tetrahydrate ($FeCl_2.4H_2O$, 99%), ferrous sulfate heptahydrate ($FeSO_4.7H_2O$, 99%), ferric chloride hexahydrate ($FeCl_3.6H_2O$, 99%), sodium borohydride ($NaBH_4$, 99%) and hydrochloric acid (HCl, 99%) were purchased from Sigma-Aldrich. Ethanol (C_2H_5OH, 99%), sodium hydroxide (NaOH, 33%), hydrazine (N_2H_4, 99%) and ammonium hydroxide (NH_4OH, 99%) were procured from Pharos company (Egypt). Silica gel (SiO_2, 99%) was purchased from Fluka in Switzerland and starch (99%) was procured from Nice Chemicals in India. Potassium dichromate ($K_2Cr_2O_7$, 97%) and humic acid ($C_9H_9NO_6$, 99%) were obtained from Sigma-Aldrich. Zinc chloride ($ZnCl_2$, 97%), magnesium chloride hexahydrate ($MgCl_2.6H_2O$, 99%), sodium nitrate ($NaNO_3$, 98%), copper chloride dihydrate ($CuCl_2.2H_2O$, 99%), sodium sulfate (Na_2SO_4, 99%), sodium phosphate dodecahydrate ($Na_3PO_4.12H_2O$, 99%) and sodium carbonate dehydrate ($Na_2CO_3.10H_2O$, 98%) were purchased from Loba Chemie (India). All chemicals were of high purity and used directly without any modifications.

Preparation of pure nano zero-valent iron (NZVI) and modified NZVI composite. NZVI was synthesized via the liquid-phase reduction method in which ferrous ions (Fe^{2+}) in an aqueous solution can be rapidly reduced to zero-valent ion (Fe^0) using sodium borohydride ($NaBH_4$) as a reducing agent as shown in Eq. (5). The optimum reaction time, reducing agent and iron salt were specified based on the results of the optimization of NZVI preparation process that were discussed in the results and discussion section.

$$Fe^{2+}_{(aq)} + 2BH^-_{4(aq)} + 6H_2O \rightarrow Fe^0_{(s)} + 2B(OH)_{3(aq)} + 7H_2 \uparrow \quad (5)$$

In detail, 1 M of $FeCl_2.4H_2O$ was added to 50 mL of ethanol. Subsequently, 4 M of $NaBH_4$ was mixed with 20 mL of distilled water and the formed solution was added dropwise (50–60 drops/min) to the ferrous solution during mixing in an aerobic condition (Without purging N_2 or Ar). The mixture color turned to black after adding the $NaBH_4$ solution affirming the reduction of ferrous ions to zero-valent iron and the mixture was further stirred for 10 min to secure the time required for the complete reduction of ferrous ions to Fe^0. Then, the particles were collected using an external magnet and washed five times with distilled water and absolute ethanol to ensure the removal of reducing agent residuals. After washing, the nanoparticles were collected by centrifugation at 6000 rpm followed by drying at 50 °C overnight in a vacuum condition.

To prepare the NZVI based composite nanomaterials through supporting on either organic starch (NZVI-St) or inorganic silica gel (NZVI-Si), the same procedures for the preparation of the bare NZVI were followed beside the addition of ferrous solution and ethanol to 0.3 g of silica gel or starch and sonication for 30 min to affirm the dispersion of supporting materials before the addition of $NaBH_4$ solution.

Experimental procedures. The preparation of NZVI was conducted at reaction times of 10, 30, 60 and 120 min using different iron salts and reducing agents under vigorous stirring. The yield of the prepared NZVI samples was estimated and the performance of the prepared NZVI for the removal of acid blue-25 was evaluated at initial dye concentration of 50 mg L^{-1}, NZVI dose of 0.1 g, solution volume of 100 mL, contact time of 60 min and agitation rate of 200 rpm. The synthesis of NZVI supported on the surface of silica or starch was performed by adding the iron solution ($FeCl_2.4H_2O$) and ethanol on the supporting material. Then, the reducing agent (sodium borohydride ($NaBH_4$)) was added to reduce iron ions to zero-valent iron supported on silica or starch. The adsorption integrated with chemical reduction of chromium Cr(VI) or acid blue-25 by the synthesized nanoparticles was conducted in a screw cap glass bottle. The bottle was filled with 100 mL of Cr(VI) or acid blue-25 dye solution and 0.1 g of the adsorbent was added at 20 °C. Then, the contaminated solution with the added adsorbent was placed in an incubator shaker for 120 min to remove Cr(VI) and 60 min for the removal of acid blue-25 (200 rpm). A stock solution of Cr(VI)) with a concentration of 1000 mg L^{-1} was prepared by dissolving 0.2829 g of $K_2Cr_2O_7$ in distilled water (1000 mL) and another stock solution of acid blue-25 dye was prepared. The pH values were adjusted using 0.1 M of NaOH or HCl and the effect of pH (1–11) was investigated as well as the effect of initial Cr(VI) concentration (5–100 mg L^{-1}) on the removal efficiency was studied at an adsorbent dose of 0.1 g, solution volume of 100 mL, contact time of 120 min, temperature of 20 °C and agitation rate of 200 rpm. The effects of the existence of cations such as Mg^{2+}, Zn^{2+} and Cu^{2+}, anions viz., NO_3^-, CO_3^{2-}, SO_4^{2-} and

PO_4^{3-} and humic acid on the removal efficacy were investigated. The concentration of anions and cations was 40 mg L^{-1} and the investigation of the effect of humic acid on the adsorption system was conducted using two concentrations of humic acid (5 mg L^{-1} and 20 mg L^{-1}) at NZVI-Si dose of 0.1 g/100 mL, pH 1, initial Cr(VI) concentration of 25 mg L^{-1}, contact time of 120 min and temperature of 20 °C. The reusability study was conducted for six cycles at NZVI-Si dose of 0.1 g/100 mL, initial Cr(VI) concentration of 25 mg/L, pH 1, contact time of 120 min, and temperature of 20 °C. The particles were collected after each cycle using a magnet, and then they were washed with water and dried for successive use. The effect of adding H_2O_2 (0.25–1 mM) on the removal performance was investigated at NZVI-Si dose of 0.1 g/100 mL, initial Cr(VI) concentration of 25 mg L^{-1}, contact time of 120 min and temperature of 20 °C. The samples were withdrawn during the contact time and centrifuged to separate the nanoparticles. Thereafter, measurement of Cr(VI) and acid blue-25 concentrations was performed using a UV spectrophotometer instrument (JASCO V-630) at 540 and 602 nm, respectively. Adsorption kinetics were studied during the time interval (0–120 min) at an initial Cr(VI) concentration of 25 mg L^{-1} and pH 1 using first-order, second-order, intraparticle diffusion, Elovich, power function, parabolic diffusion and Boyd kinetic models and investigation of the adsorption equilibrium was conducted at initial Cr(VI) concentrations of 5, 10, 25, 50 and 100 mg L^{-1}, pH 1 and time of 120 min using Langmuir, Freundlich, Dubinin-Radushkevish, Temkin, Harkins–Jura and Generalized isotherm models. Thermodynamic study was performed at different temperatures (293, 313, 328, 343 and 358 K). The equations and discussion of kinetic, thermodynamic and isotherm models were provided in the supplementary file (Text S1).

The removal percentage of Cr(VI) or acid blue-25 dye was calculated as shown in Eq. (6):

$$\text{Removal } \% \; = \; ((C_o - C_e)/C_o) \; * 100 \tag{6}$$

where C_o is the initial Cr(VI) or dye concentration (mg L^{-1}) and C_e is the Cr(VI) or dye concentration at equilibrium (mg L^{-1}). The adsorption capacities of the synthesized materials were calculated using Eq. (7):

$$q_e \; = \; V \; (C_o - C_e)/m \tag{7}$$

where q_e is the adsorption capacity of the synthesized materials at equilibrium (mg g^{-1}); V is the solution volume (L); and m is the mass of synthesized nanomaterials (g).

Analytical methods. The diffraction planes of the synthesized nanomaterials were specified using X-ray diffraction analysis (XRD, Siemens model D-5000 diffractometer). The morphology, crystallinity, and chemical composition of the synthesized materials were investigated by performing transmission electron microscopy (TEM) coupled with energy dispersive X-ray spectroscopy (EDS), elemental mapping and selected area electron diffraction (SAED) (JEOL JEM-2100). The chemical bonds existing in the synthesized nanomaterials were specified using Fourier transform infrared spectroscopy (Shimadzu, FTIR-8400S). The surface area and pore size distribution of the synthesized nanomaterials were estimated using Belsorp-max automated apparatus (BEL Japan). Moreover, the chemical composition and oxidation states of the prepared nanoparticles were studied by performing an X-ray photoelectron spectroscopy analysis (Thermo-Fisher, USA). The magnetic characteristics of the synthesized nanomaterials were evaluated using vibrating sample magnetometer (VSM, Lake Shore-7410, USA), magnetic field up to 20 kOe and the sensitivity up to 1 μ emu. The point of zero charge was estimated using solid addition method as reported in our previous work[56].

Conclusions

Sodium borohydride and ferrous chloride tetrahydrate were the optimum reducing agent and iron precursor, respectively for the preparation of pure NZVI after a reaction time of 10 min. The NZVI surface was modified it by supporting on starch or silica gel. The excellent support on modifiers was confirmed by various analyses such as TEM, EDS and XPS. The optimized NZVI can attain full removal of acid blue-25 dye after 60 min. NZVI-Si showed higher performance than pure NZVI and NZVI-St. The adsorption capacity was improved at elevated concentrations of Cr(VI) under acidic conditions. Adsorption kinetics, isotherms and thermodynamics studies indicated that the adsorption process was physical, favorable, spontaneous and endothermic. The existence of cations such as Mg^{2+}, Zn^{2+} and Cu^{2+} and anions like NO_3^-, CO_3^{2-}, SO_4^{2-}, PO_4^{3-} decreased the removal efficiency of Cr(VI). The addition of alow concentration of HA (5 mg L^{-1}) can improve the removal efficiency compared to reduced removal performance at high HA concentration (10 mg L^{-1}). The addition of H_2O_2 with a concentration over 0.75 mM reduced the removal efficiency. The removal efficiencies were 96.8%, 93.67%, 90.1%, 86.7, 82.9% and 74.8% after six repetitive cycles using NZVI-Si. Reduction, adsorption and precipitation were the major removal Cr(VI) mechanisms onto the prepared NZVI-Si.

Data availability

The data that support the findings of this study are available from the corresponding author upon reasonable request.

Received: 22 October 2022; Accepted: 16 December 2022
Published online: 23 December 2022

References

1. Chen, Y. H. & Huang, P. J. Sono-assisted rapid dye removal by chromium-based metal organic frameworks derived from waste PET bottles: Characterization, kinetics and adsorption isotherms. *J. Environ. Chem. Eng.* **9**, 106766 (2021).
2. Jaiyeola, O. O., Chen, H., Albadarin, A. B. & Mangwandi, C. Production of bio-waste granules and their evaluation as adsorbent for removal of hexavalent chromium and methylene blue dye. *Chem. Eng. Res. Des.* **164**, 59–67 (2020).

3. Qiu, J. *et al.* Recyclable Nanocomposite of Flowerlike MoS2@Hybrid Acid-Doped PANI Immobilized on Porous PAN Nanofibers for the Efficient Removal of Cr(VI). *ACS Sustain. Chem. Eng.* **6**, 447–456 (2018).
4. Elkady, M., Shokry, H., El-Sharkawy, A., El-Subruiti, G. & Hamad, H. New insights into the activity of green supported nanoscale zero-valent iron composites for enhanced acid blue-25 dye synergistic decolorization from aqueous medium. *J. Mol. Liq.* **294**, 111628 (2019).
5. Chen, Z. *et al.* Synthesis of PANI/AlOOH composite for Cr(VI) adsorption and reduction from aqueous solutions. *ChemistrySelect* **4**, 2352–2362 (2019).
6. Rai, M. K. *et al.* Adsorption of hexavalent chromium from aqueous solution by activated carbon prepared from almond shell: Kinetics, equilibrium and thermodynamics study. *J. Water Supply Res. Technol. - AQUA* **67**, 724–737 (2018).
7. Yao, Y. *et al.* A novel colloid composited with polyacrylate and nano ferrous sulfide and its efficiency and mechanism of removal of Cr(VI) from Water. *J. Hazard. Mater.* **399**, (2020).
8. Hsini, A. *et al.* Synthesis of an arginine-functionalized polyaniline@FeOOH composite with high removal performance of hexavalent chromium ions from water: Adsorption behavior, regeneration and process capability studies. *Colloids Surfaces A Physicochem. Eng. Asp.* **617**, 126274 (2021).
9. Karthik, R. & Meenakshi, S. Removal of hexavalent chromium ions using polyaniline/silica gel composite. *J. Water Process Eng.* **1**, 37–45 (2014).
10. Sriram, G. *et al.* Recent trends in the application of metal-organic frameworks (MOFs) for the removal of toxic dyes and their removal mechanism-a review. *Sustain. Mater. Technol.* **31**, (2022).
11. Hamad, H. *et al.* The superior photocatalytic performance and DFT insights of S-scheme CuO@TiO_2 heterojunction composites for simultaneous degradation of organics. *Sci. Rep.* **12**, 2217 (2022).
12. Ramírez-Estrada, A. *et al.* Cr(III) removal from synthetic and real tanning effluents using an electro-precipitation method. *J. Environ. Chem. Eng.* **6**, 1219–1225 (2018).
13. Mukherjee, R., Bhunia, P. & De, S. Long term filtration modelling and scaling up of mixed matrix ultrafiltration hollow fiber membrane: a case study of chromium(VI) removal. *J. Memb. Sci.* **570–571**, 204–214 (2019).
14. El-Ashtoukhy, E-S.Z., Amin, N. K., Fouad, Y.O., & Hamad. H.A. Intensification of a new electrocoagulation system characterized by minimum energy consumption and maximum removal efficiency of heavy metals from simulated wastewater. *Chem. Eng. Process: Process Intensif.154*, 108026 (2020).
15. Eltarahony, M., Abu-Serie, M., Hamad, H., Zaki, S. & Abd-El-Haleem, D. Unveiling the role of novel biogenic functionalized CuFe hybrid nanocomposites in boosting anticancer, antimicrobial and biosorption activities. *Sci. Rep.* **11**, 7790 (2021).
16. Samy, M., Gar Alalm, M., Fujii, M. & Ibrahim, M. G. Doping of Ni in MIL-125(Ti) for enhanced photocatalytic degradation of carbofuran: Reusability of coated plates and effect of different water matrices. *J. Water Process Eng.* **44**, 102449 (2021).
17. Samy, M. *et al.* CNTs / MOF-808 painted plates for extended treatment of pharmaceutical and agrochemical wastewaters in a novel photocatalytic reactor. *Chem. Eng. J.* **406**, 7 (2021).
18. Samy, M., Alalm, M. G. & Mossad, M. Utilization of iron sludge resulted from electro-coagulation in heterogeneous photo-fenton process. *Water Pract. Technol.* **15**, 1228–1237 (2020).
19. Samy, M., Ibrahim, M. G., Alalm, M. G. & Fujii, M. Modeling and Optimization of Photocatalytic Degradation of Methylene Blue Using Lanthanum Vanadate. **1008**, 97–103 (2020).
20. Lei, C., Wang, C., Chen, W., He, M. & Huang, B. Polyaniline@magnetic chitosan nanomaterials for highly efficient simultaneous adsorption and in-situ chemical reduction of hexavalent chromium: Removal efficacy and mechanisms. *Sci. Total Environ.* **733**, 139316 (2020).
21. El-Sayed, E. M., Hamad, H. A. & Ali, R. M. Journey from ceramic waste to highly efficient toxic dye adsorption from aqueous solutions via one-pot synthesis of $CaSO_4$ rod-shape with silica. *J. Mater. Res. Technol.* **6**, 16051–16063 (2020).
22. Vilardi, G., Sebastiani, D., Miliziano, S., Verdone, N. & Di Palma, L. Heterogeneous nZVI-induced Fenton oxidation process to enhance biodegradability of excavation by-products. *Chem. Eng. J.* **335**, 309–320 (2018).
23. Donadelli, J. A., Carlos, L., Arques, A. & García Einschlag, F. S. Kinetic and mechanistic analysis of azo dyes decolorization by ZVI-assisted Fenton systems: pH-dependent shift in the contributions of reductive and oxidative transformation pathways. *Appl. Catal. B Environ.* **231**, 51–61 (2018).
24. Niu, H. *et al.* Single-crystalline Fe7S8/Fe3O4 coated zero-valent iron synthesized with vacuum chemical vapor deposition technique: Enhanced reductive, oxidative and photocatalytic activity for water purification. *J. Hazard. Mater.* **401**, 123442 (2021).
25. Phenrat, T. *et al.* Stabilization of aqueous nanoscale zerovalent iron dispersions by anionic polyelectrolytes: Adsorbed anionic polyelectrolyte layer properties and their effect on aggregation and sedimentation. *J. Nanoparticle Res.* **10**, 795–814 (2008).
26. Ma, Q. *et al.* Multi-component removal of Pb(II), Cd(II), and As(V) over core-shell structured nanoscale zero-valent iron@ mesoporous hydrated silica. *Sci. Total Environ.* **827**, 154329 (2022).`using MD simulation. *Int. J. Biol. Macromol.* **121**, 727–733 (2019).
27. Xu, M. *et al.* Spectroscopic investigation of Cr(VI) sorption on nZVI/biochar composites. *J. Mol. Liq.* **366**, 120262 (2022).
28. Bao, T. *et al.* Bentonite-supported nano zero-valent iron composite as a green catalyst for bisphenol A degradation: Preparation, performance, and mechanism of action. *J. Environ. Manage.* **260**, (2020).
29. Wang, J., Liu, G., Zhou, C., Li, T. & Liu, J. Synthesis, characterization and aging study of kaolinite-supported zero-valent iron nanoparticles and its application for Ni(II) adsorption. *Mater. Res. Bull.* **60**, 421–432 (2014).
30. Silva-Calpa, L. de R. *et al.* Stable and highly active zero-valent iron-nickel nanofilaments/silica for the hexavalent chromium reduction. *Environ. Nanotechnology, Monit. Manag.* **14**, 100332 (2020).
31. Kumari, B. & Dutta, S. Integrating starch encapsulated nanoscale zero-valent iron for better chromium removal performance. *J. Water Process Eng.* **37**, 101370 (2020).
32. Sahu, M. K., Patel, R. K. & Kurwadkar, S. Mechanistic insight into the adsorption of mercury (II) on the surface of red mud supported nanoscale zero-valent iron composite. *J. Contam. Hydrol.* **246**, 103959 (2022).
33. Maamoun, I. *et al.* Multi-functional magnesium hydroxide coating for iron nanoparticles towards prolonged reactivity in Cr(VI) removal from aqueous solutions. *J. Environ. Chem. Eng.* **10**, 107431 (2022).
34. Maamoun, I. *et al.* Bench-scale injection of magnesium hydroxide encapsulated iron nanoparticles (nFe^0@$Mg(OH)_2$) into porous media for Cr(VI) removal from groundwater. *Chem. Eng. J.* **451**, 138718 (2023).
35. Wang, Q. *et al.* Mechanically activated zero-valent silicon by coating silica to decolorize Acid Red 73 dye. *Colloids Surfaces A Physicochem. Eng. Asp.* **626**, 127020 (2021).
36. Diao, Z. H. *et al.* Removals of Cr(VI) and Cd(II) by a novel nanoscale zero valent iron/peroxydisulfate process and its Fenton-like oxidation of pesticide atrazine: Coexisting effect, products and mechanism. *Chem. Eng. J.* **397**, 125382 (2020).
37. Guo, S. *et al.* Simultaneous reduction of Cr(VI) and degradation of tetracycline hydrochloride by a novel iron-modified rectorite composite through heterogeneous photo-Fenton processes. *Chem. Eng. J.* **393**, 124758 (2020).
38. Maamoun, I., Eljamal, R., Sugiharad, Y. & Eljamal, O. Statistical optimization of nZVI chemical synthesis approach towards P and NO_3^- removal from aqueous solutions: cost-effectiveness & parametric effects. *Chemosphere* **312**, 137176 (2023).
39. Mensah, K., Samy, M., Ezz, H., Elkady, M. & Shokry, H. Utilization of iron waste from steel industries in persulfate activation for effective degradation of dye solutions. *J. Environ. Manage.* **314**, 115108 (2022).
40. Wang, Y., Zhao, D., Feng, S., Chen, Y. & Xie, R. Ammonium thiocyanate functionalized graphene oxide-supported nanoscale zero-valent iron for adsorption and reduction of Cr(VI). *J. Colloid Interface Sci.* **580**, 345–353 (2020).

41. Hamadi, A., Yeddou-Mezenner, N., Azeddine, L., Ali, R. M. & Hamd, H. Upgrading of agro-industrial green biomass residues from chocolate industry for adsorption process: diffusion and mechanistic insights. *J. Food Sci. Technol.* **58**, 1081–1092 (2021).
42. Ratanaphain, C. *et al.* Reactivity characterization of SiO2-coated nano zero-valent iron for iodoacetamide degradation: The effects of SiO2 thickness, and the roles of dehalogenation, hydrolysis and adsorption. *Chemosphere* **286**, 131816 (2022).
43. Hamad, H.A., AbdElhafez, S.E., Elsenety, M. M., Sorour, M.K., Amin, N.K., Abdelwahab, O., El-Ashtoukhy, E-S.Z. Fabrication and characterization of functionalized lignin-based adsorbent prepared from black liquor in the paper industry for superior removal of toxic dye. *Fuel* **323**, 124288 (2022)
44. Rončević, S., Nemet, I., Ferri, T. Z. & Matković-Čalogović, D. Characterization of nZVI nanoparticles functionalized by EDTA and dipicolinic acid: A comparative study of metal ion removal from aqueous solutions. *RSC Adv.* **9**, 31043–31051 (2019).
45. Hamad, H. *et al.* Functionalized cellulose for the controlled synthesis of novel carbon-ti nanocomposites: Physicochemical and photocatalytic properties. *Nanomaterials* **10**, 729 (2020).
46. Liu, S. *et al.* Study on influencing factors and mechanism of removal of Cr(VI) from soil suspended liquid by bentonite-supported nanoscale zero-valent iron. *Sci. Rep.* **10**, 1–12 (2020).
47. Zhang, Q. *et al.* Chromium(VI) removal from synthetic solution using novel zero-valent iron biochar composites derived from iron-rich sludge via one-pot synthesis. *J. Water Process Eng.* **47**, 102720 (2022).
48. Zhang, S. H. *et al.* Mechanism investigation of anoxic Cr(VI) removal by nano zero-valent iron based on XPS analysis in time scale. *Chem. Eng. J.* **335**, 945–953 (2018).
49. Zhang, S. *et al.* Mechanism investigation of anoxic Cr (VI) removal by nano zero-valent iron based on XPS analysis in time scale. *Chem. Eng. J.* **335**, 945–953 (2018).
50. Wen, J., Fu, W., Ding, S., Zhang, Y. & Wang, W. Pyrogallic acid modified nanoscale zero-valent iron efficiently removed Cr (VI) by improving adsorption and electron selectivity. *Chem. Eng. J.* 136510 (2022) https://doi.org/10.1016/j.cej.2022.136510.
51. Fu, R. *et al.* The removal of chromium (VI) and lead (II) from groundwater using sepiolite-supported nanoscale zero-valent iron (S-NZVI). *Chemosphere* **138**, 726–734 (2015).
52. Dong, H. *et al.* Stabilization of nanoscale zero-valent iron (nZVI) with modified biochar for Cr(VI) removal from aqueous solution. *J. Hazard. Mater.* **332**, 79–86 (2017).
53. Zhou, H. *et al.* Sodium citrate and biochar synergistic improvement of nanoscale zero-valent iron composite for the removal of chromium (VI) in aqueous solutions. *J. Environ. Sci. (China)* **115**, 227–239 (2022).
54. Chen, W. F., Wang, W., Zhang, J., Zhang, X. & Li, Y. Effects of co-present cations and anions on hexachlorobenzene removal by activated carbon, nano zerovalent iron and nano zerovalent/activated carbon composite. *Desalin. Water Treat.* **57**, 20494–20502 (2016).
55. Lv, X. *et al.* Effects of co-existing ions and natural organic matter on removal of chromium (VI) from aqueous solution by nanoscale zero valent iron (nZVI)-Fe3O4 nanocomposites. *Chem. Eng. J.* **218**, 55–64 (2013).
56. Abdelkhalek, A., El-Latif, M. A., Ibrahim, H., Hamad, H. & Showman, M. Controlled synthesis of graphene oxide/silica hybrid nanocomposites for removal of aromatic pollutants in water. *Sci. Rep.* **12**, 7060 (2022).
57. Tarekegn, M. M., Hiruy, A. M. & Dekebo, A. H. Nano zero valent iron (nZVI) particles for the removal of heavy metals (Cd^{2+}, Cu^{2+} and Pb^{2+}) from aqueous solutions. *RSC Adv.* **11**, 18539–18551 (2021).
58. Boparai, H. K., Joseph, M. & O'Carroll, D. M. Cadmium (Cd^{2+}) removal by nano zerovalent iron: Surface analysis, effects of solution chemistry and surface complexation modeling. *Environ. Sci. Pollut. Res.* **20**, 6210–6221 (2013).
59. Boparai, H. K., Joseph, M. & O'Carroll, D. M. Kinetics and thermodynamics of cadmium ion removal by adsorption onto nano zerovalent iron particles. *J. Hazard. Mater.* **186**, 458–465 (2011).
60. Sun, X. *et al.* Nanoscale zero-valent iron immobilized inside the mesopores of ordered mesoporous carbon by the " two solvents " reduction technique for Cr (VI) and As (V) removal from aqueous solution. *J. Mol. Liq.* **315**, 113598 (2020).
61. Samy, M., Ibrahim, M. G., Gar, M. & Fujii, M. MIL-53 (Al)/ ZnO coated plates with high photocatalytic activity for extended degradation of trimethoprim via novel photocatalytic reactor. *Sep. Purif. Technol.* **249**, 117173 (2020).

Acknowledgements

The authors are deeply grateful to the City of Scientific Research and Technological Applications (SRTA-City), Egypt-Japan University of Science and Technology (E-JUST), Mansoura University, and the Alexandria University in Egypt. The second author is supported by Faculty of Engineering, Mansoura University.

Author contributions

E.S.: Methodology, Investigation, Validation, Formal analysis, Visualization; M.S.: Investigation, Validation, Formal analysis, Visualization, Data Curation, Writing–original draft; H.S.: Investigation, Validation, Formal analysis, Data Curation; G.E.-S.: Investigation, Validation, Formal analysis, Data Curation; A.E.-S.: Methodology, Investigation, Validation, Formal analysis, Visualization H.H.: Conceptualization, Investigation, Validation, Formal analysis, Visualization, Data Curation; Writing-reviewing & editing, Resources, Supervision, Project administration; M.E.: Conceptualization, Investigation, Validation, Formal analysis, Visualization, Data Curation, Writing –original draft, Resources, Supervision, Project administration.

Funding

Open access funding provided by The Science, Technology & Innovation Funding Authority (STDF) in cooperation with The Egyptian Knowledge Bank (EKB).

Competing interests

The authors declare no competing interests.

Additional information

Supplementary Information The online version contains supplementary material available at https://doi.org/10.1038/s41598-022-26612-1.

Correspondence and requests for materials should be addressed to H.H. or M.E.